May 30, 1999 CB-note 344

Technical Report:

$\bar{p}p$ annihilation at rest into two-body final states and branching ratios (LH_2)

Burkhard Pick

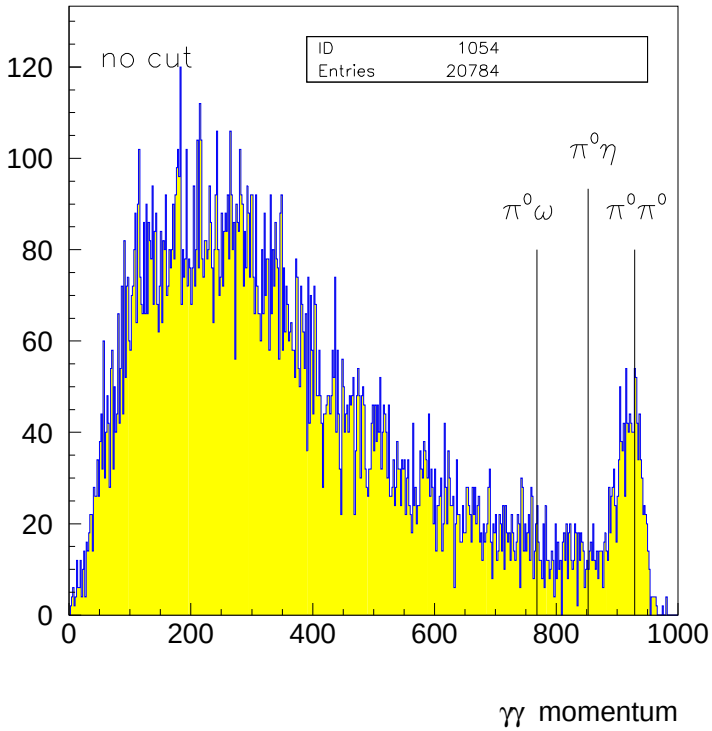

Institut für Strahlen– und Kernphysik, Universität Bonn, D–53115 Bonn

http://www.iskp.uni-bonn.de/cbiskp/cbiskp.html

Contents

Chapter 1

Introduction

In 1993 the Crystal Barrel Collaboration published the $\bar{p}p \to \pi^0\pi^0$ branching ratio in liquid hydrogen at rest [2]

$$BR(\bar{p}p \to \pi^0\pi^0) = (6.93 \pm 0.43) \cdot 10^{-4} \tag{1.1}$$

At HADRON'97 the OBELIX Collaboration presented their new measurement:

$$BR(\bar{p}p \to \pi^0\pi^0) = (2.8 \pm 0.4) \cdot 10^{-4} \tag{1.2}$$

Because of this discrepancy of a factor of 2.5 Chris Batty and myself are in contact with A. Zoccoli from OBELIX. We would like to find the reason for the different values.

The branching ratio for $\bar{p}p \to K_S K_L$ was determined by the OBELIX experiment. Their value $(7.8 \pm 0.8) \cdot 10^{-4}$ [8] is compatible to our result $(9.0 \pm 0.6) \cdot 10^{-4}$ [7]. They looked for K_S decaying into $\pi^+\pi^-$ whereas we searched for the $\pi^0\pi^0$ decay mode. This could be a hint that their detection efficiency for γ's is not correct.

In order to improve this, minimum bias data taken in April 96, not being part of our previous publication, was analysed without applying a kinematical fit as it was done before. All steps are done as simple as possible to avoid side effects by the selection.

The branching ratios for $\bar{p}p \to \pi^0\pi^0$, $\pi^0\eta$ and $K_L^{miss}K_S$ ($K_S \to \pi^0\pi^0$) in LH_2 are presented.

$\bar{p}p$-annihilation at rest into two mesons is restricted by conservation laws: parity P, C-parity and the angular momentum are conserved in strong interaction processes. Therefore only a limited number of partial waves contributes to the annihilation.

The $\pi^0\pi^0$, $\pi^0\eta$ and $\eta\eta$ final states are forbidden from initial S-states but allowed from $^3P_0$ and $^3P_2$. Therefore, these branching ratios are used to determine the P-state annihilation fraction f_P. In contrast to this the annihilation into $K_L K_S$ final-state is only allowed from $^3S_1$ initial-state. Table 1.1 gives a survey of the allowed $\bar{p}p$ initial-states for two-body reactions.

In table 1.2 the momenta for all reactions studied in this analysis are listed.

In the analysis presented here branching ratios in liquid hydrogen have been determined. A similar analysis based on data taken with a gaseous hydrogen target will follow soon.

$\bar{p}p \rightarrow$	Allowed initial states		
$\pi^0\pi^0$		$^3P_0$	$^3P_2$
$\pi^+\pi^-$	$^3S_1$	$^3P_0$	$^3P_2$
K_SK_L	$^3S_1$		
K_SK_S		$^3P_0$	$^3P_2$
K^+K^-	$^3S_1$	$^3P_0$	$^3P_2$

Table 1.1: Allowed $\bar{p}p$ initial-states for two-body reactions.

Channel	Momentum	Channel	Momentum
$\pi^+\pi^-$	927.8 MeV/c	$\pi^0\omega$	768.4 MeV/c
K^+K^-	797.9 MeV/c	$\pi^0\eta'$	658.7 MeV/c
$\pi^0\pi^0$	928.5 MeV/c	$\eta\eta$	761.0 MeV/c
$\pi^0\eta$	852.3 MeV/c	$\eta\eta'$	546.1 MeV/c
K_LK_S	795.4 MeV/c		

Table 1.2: Momenta for $\bar{p}p$-annihilation into two mesons.

Chapter 2

The April 1996 minimum bias data

The analysis discussed in this report is based on the runs (LH_2 target) listed below. Up to run 36023 the trigger file was called `minbias.default` and afterwards `mbk.default`.

34702 GK0395	35061 GK0404	35457 GK0412	35955 GK0422
34703 GK0395	35088 GK0405	35477 GK0412	35957 GK0422
34724 GK0395	35178 GK0407	35482 GK0412	35978 GK0422
34729 GK0395	35192 GK0408	35506 GK0413	36000 GK0423
34737 GK0395	35220 GK0408	35507 GK0413	36023 GK0423
34751 GK0396	35239 GK0408	35508 GK0413	36047 GK0424
34753 GK0396	35260 GK0409	35526 GK0413	36055 GK0424
34765 GK0396	35263 GK0409	35584 GK0414	36069 GK0424
34777 GK0396	35266 GK0409	35585 GK0414	36094 GK0425
34795 GK0397	35293 GK0409	35586 GK0414	36128 GK0426
34808 GK0397	35301 GK0409	35641 GK0415	36155 GK0427
34840 GK0398	35342 GK0410	35711 GK0416	36182 GK0427
34856 GK0398	35390 GK0411	35801 GK0418	36215 GK0428
34870 GK0399	35402 GK0411	35848 GK0419	36240 GK0429
34942 GK0401	35432 GK0412	35871 GK0420	36258 GK0429
35010 GK0403	35433 GK0412	35922 GK0421	
35058 GK0404	35436 GK0412	35934 GK0421	

The total number of physical events is 1 801 267. Excluding events with pile-up flag reduces the number to 1 591 407. Figure 2.1a) shows the number of particles, figure 2.1b) the number of PEDs and figure 2.1c) the number of charged particles per event.

Figure 2.2 shows an unfolded view on the calorimeter for all events containing no charged tracks. The energy for all γ's (including split offs) is summed up in figure 2.3. After rejection of split off events the γ distribution looks like shown in figure 2.4. The momentum of all γ's vs. the total energy is plotted in figure 2.5.

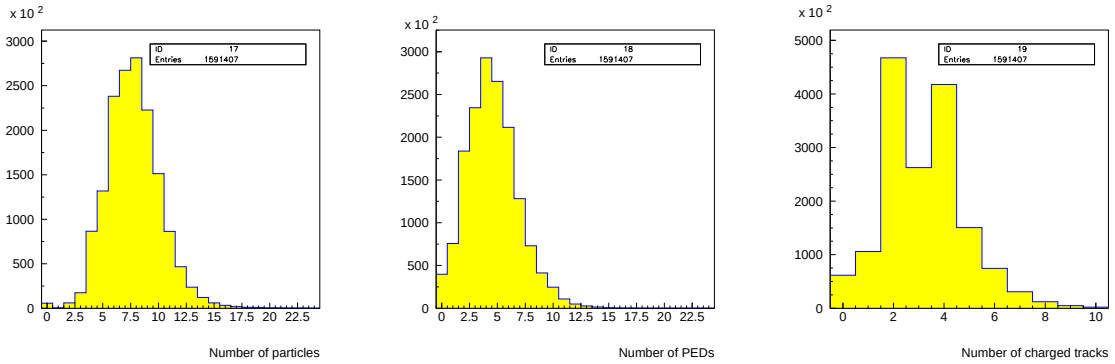

Figure 2.1: The number of particles, PEDs and charged tracks for each event (1 591 407 events).

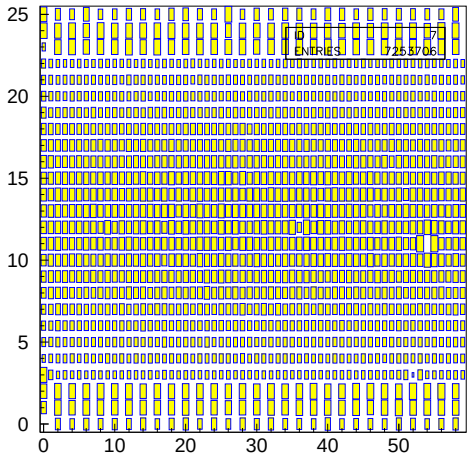

Figure 2.2: Unfolded view of the calorimeter.

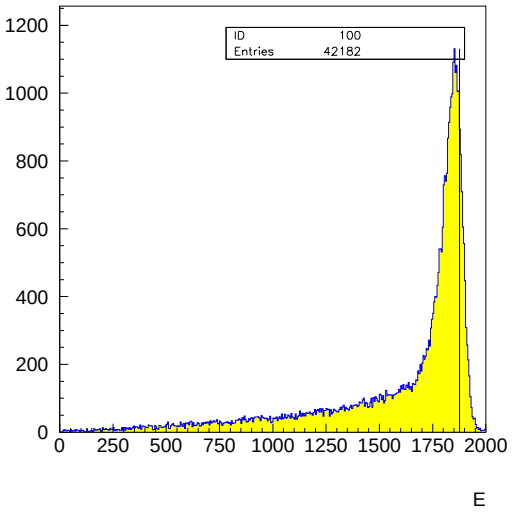

Figure 2.3: Energy of all γ's.

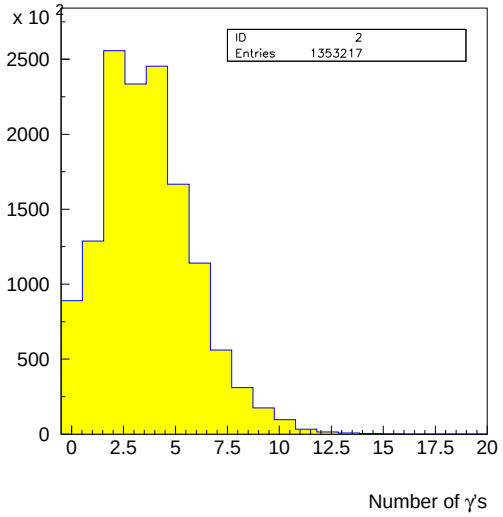

Figure 2.4: Number of γ's per event after split off rejection.

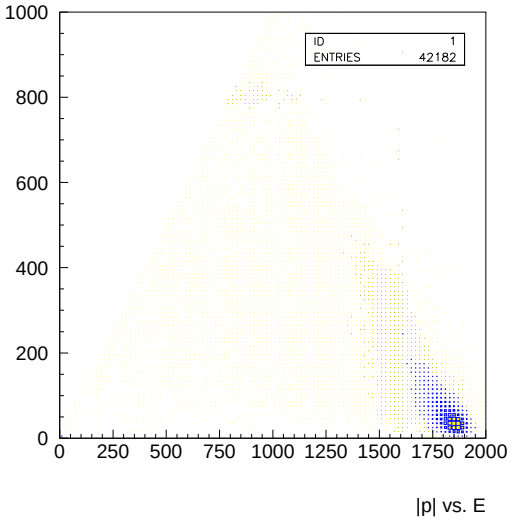

Figure 2.5: $|\vec{p}|$ vs. E

2.1 Annihilation outside the target

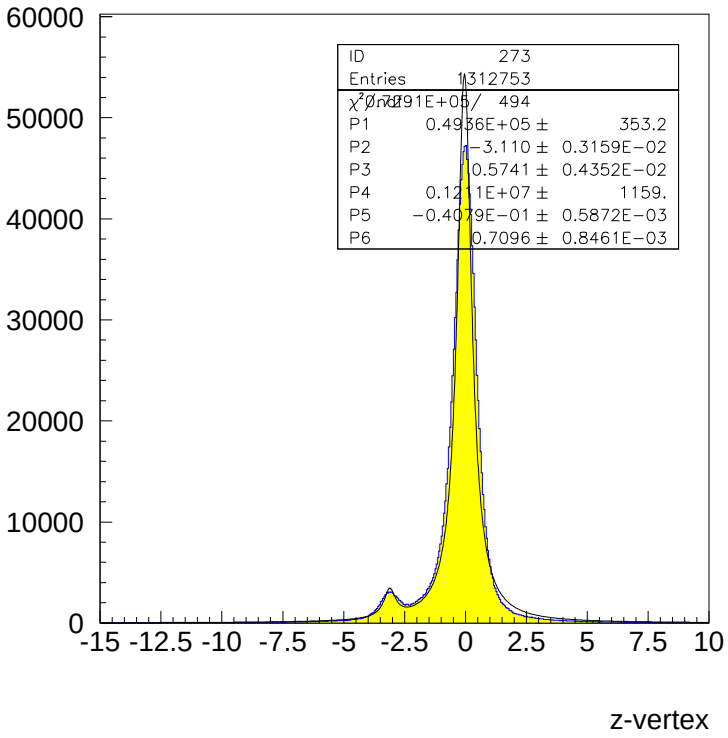

Figure 2.6: Vertex z distribution for charged tracks.

The z-vertex distribution in figure 2.6 for events containing charged tracks shows a large peak in the center and a smaller one at $z = -3.1\,\text{cm}$ not related to stops in the target. Therefore, the total number of events must be corrected. The lineshape in figure 2.6 is fitted with two Breit-Wigner functions and the result is given in table 2.1.

The total number of events containing charged tracks is 1 312 753. $49\,360 \pm 353$ of them are related to annihilations around $z = -3.1\,\text{cm}$. A fit yields $(3.7 \pm 0.7)\%$ of the events annihilating outside the target.

function	1			2		
	N	z	σ	N	z	σ
BW(1)+BW(2)	$49\,360 \pm 353$	-3.1	0.6	$1\,210\,900 \pm 1\,172$	-0.04	0.7

Table 2.1: Annihilation outside the target. The total number of events containing charged tracks is 1 312 753.

Chapter 3

In-flight annihilation

In [2] was found that $(5.7 \pm 1.1)\%$ of events annihilate in-flight. In that work the vertex distribution for $\pi^0\pi^0$ events was fitted kinematically requiring the following constraints:

$$p_x = p_y = 0 \qquad \text{and} \qquad E_{\text{tot}} = 1876.54\,\text{MeV} \tag{3.1}$$

The result was a prominent peak for $p_z = 0$ and a small peak around a mean momentum $p_z = 105\,\text{MeV}/c$. A 6C kinematic fit reduces the amount of $\bar{\text{p}}\text{p}$ annihilating in-flight to $(0.6 \pm 0.6)\%$. For more details see [3] and [4].

The analysis method used in this work is much simpler. Here no kinematic fit is applied. Thus, the final two-body events include in-flight annihilation as well as the reference data set (minimum bias events). Assuming the branching ratio does not change for in-flight annihilation at very low momenta this effect cancels out.

Chapter 4

The Monte Carlo data

In order to the determine the different detection efficiencies Monte Carlo events have been produced for every channel. For this purpose the CBGEANT version 5.05/11 and GEANT version Version 3.21/07 was used. These events are submitted to the same reconstruction software as the real data.

The K_L was produced as a non-interacting missing particle decaying immediately into two geantinos ($\tau = 10^{-20}$ sec).

A list of the produced Monte Carlo events is given in table 4.1. All produced Monte Carlo π^0's decay into $\gamma\gamma$ (98.802%) and the η's into $\gamma\gamma$ (100%).

final state	CBGEANT particle id	number of events
$\pi^0\pi^0$	7, 7	600 000
$\pi^0\eta$	7, 62	600 000
$(K_S \to \pi^0\pi^0)K_L^{missing}$		600 000
$\pi^+\pi^-$	8, 9	600 000
K^+K^-	11, 12	600 000
$(\omega \to \pi^0\gamma)\pi^0$	7, 68	455 469

Table 4.1: List of produced Monte Carlo data.

Chapter 5

4-γ events

The following definition for a reconstructed γ is applied:

- `ECLUBC = 14. EPEDBC = 13. ECLSBC = 13.`
- E1/E9 > 0.96
- TAXI and DOLBY-C
- energy of central crystal 10 MeV
- no crystal type 13

From all events remaining after the preselection the 4-γ events are selected and the momenta and invariant masses of all six $\gamma\gamma$ combinations are calculated. Figure 5.1 shows the $\gamma\gamma$ momentum for all combinations. This is the essential plot for the determination of the branching ratios. Every $\pi^0\pi^0$ causes two entries in the peak on the right side. A simple way to improve the resolution of the $\gamma\gamma$ momenta, e.g. the sum of the momenta of γ_1 and γ_2, is ($\sum_{i=1}^{4} \vec{p}_i = 0$)

$$\vec{p}_1 + \vec{p}_2 = -\frac{1}{2}(\vec{p}_3 + \vec{p}_4 - \vec{p}_1 - \vec{p}_2) \tag{5.1}$$

It is very difficult to find the correct description for the background. On the right side of the left picture one can see a small peak for the $\bar{\mathrm{p}}\mathrm{p} \to \pi^0\eta$ final state and a larger one for $\bar{\mathrm{p}}\mathrm{p} \to \pi^0\omega$ where one soft γ is lost.

The invariant masses of all two-γ-combinations are in figure 5.1. A large peak for π^0- and a smaller one for η-events is visible.

A very simple way to suppress the background from other channels is the following requirement. The invariant mass of the $\gamma\gamma$-combination for each particle must be in an interval around the particle mass m_i.

$$|m(\gamma\gamma) - m_i| < 50\,\mathrm{MeV} \tag{5.2}$$

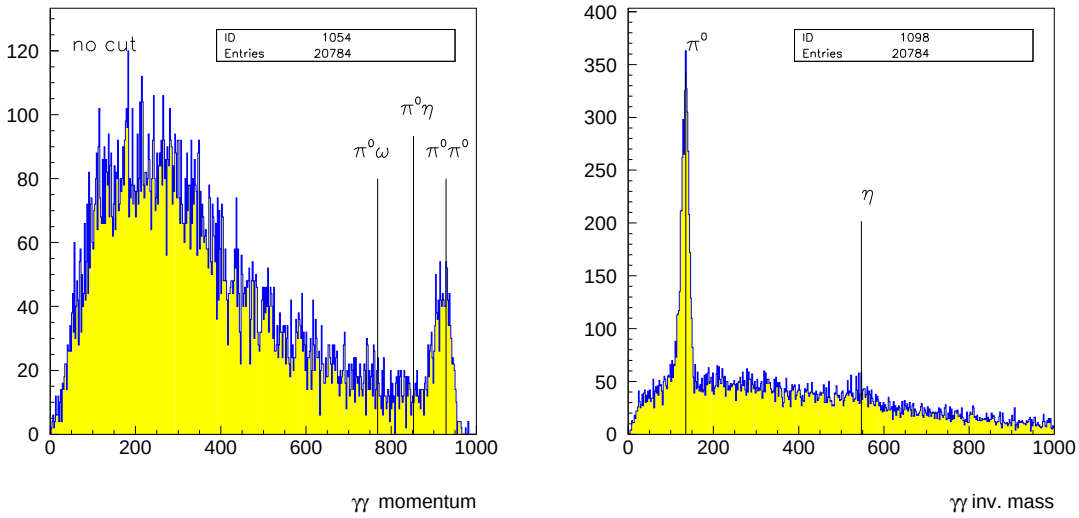

Figure 5.1: (left) Momentum of all six 2-γ combinations. Each $\pi^0\pi^0$ event causes two entries in the peak on the right side.
(right) Invariant mass of all six 2-γ combinations.

On the one hand the background will be reduced but on the other hand double counting can occur. Exactly none or one $\gamma\gamma$ combination must be found. From all six $\gamma\gamma$-combinations the one with the lowest distance d to the masses of the desired particles m_a and m_b will be chosen.

$$d = |m_i(\gamma\gamma) - m_a| + |m_j(\gamma\gamma) - m_b| \tag{5.3}$$

Furthermore, this event must comply with (5.2).

An additional method to understand the background shows figure 5.2. The $|\vec{p}|$ versus E distribution is separated into different regions. So the influence of missing momentum and missing energy can be studied. The kinematic conditions are listed in table 5.1.

A	$1700\text{MeV}/c - E < \vert\vec{p}\vert < 2000\text{MeV}/c - E$ $\vert\vec{p}\vert < -150\text{MeV}/c + 0.3E$
B	$1700\text{MeV}/c - E < \vert\vec{p}\vert < 2000\text{MeV}/c - E$ $\vert\vec{p}\vert < -200\text{MeV}/c + 0.3E$
C	$1700\text{MeV}/c - E < \vert\vec{p}\vert < 2000\text{MeV}/c - E$ $\vert\vec{p}\vert < -250\text{MeV}/c + 0.3E$
D	$1700\text{MeV}/c - E < \vert\vec{p}\vert < 2000\text{MeV}/c - E$ $\vert\vec{p}\vert < -300\text{MeV}/c + 0.3E$
E	$1700\text{MeV}/c - E < \vert\vec{p}\vert < 2000\text{MeV}/c - E$ $\vert\vec{p}\vert < -350\text{MeV}/c + 0.3E$
F	$1700\text{MeV}/c - E < \vert\vec{p}\vert < 2000\text{MeV}/c - E$ $\vert\vec{p}\vert < -400\text{MeV}/c + 0.3E$
G	$1700\text{MeV}/c - E < \vert\vec{p}\vert < 2000\text{MeV}/c - E$ $\vert\vec{p}\vert < -450\text{MeV}/c + 0.3E$
large box H	$\vert\vec{p}\vert < 300\text{MeV}/c$ $1500\,\text{MeV}/c^2 < E < 2000\,\text{MeV}/c^2$
small box I	$\vert\vec{p}\vert < 90\text{MeV}/c$ $1700\,\text{MeV}/c^2 < E < 2000\,\text{MeV}/c^2$
$\text{K}_\text{L}^\text{miss}$ J	$0.8E < \vert\vec{p}\vert < E$ $\vert\vec{p}\vert > -E + 1550\text{MeV}/c^2$ $\vert\vec{p}\vert < -E + 1900\text{MeV}/c^2$
$\text{K}_\text{L}^\text{miss}$ K	$0.81E < \vert\vec{p}\vert < 0.975E$ $\vert\vec{p}\vert > -E + 1575\text{MeV}/c^2$ $\vert\vec{p}\vert < -E + 1875\text{MeV}/c^2$
$\text{K}_\text{L}^\text{miss}$ L	$0.82E < \vert\vec{p}\vert < 0.95E$ $\vert\vec{p}\vert > -E + 1600\text{MeV}/c^2$ $\vert\vec{p}\vert < -E + 1850\text{MeV}/c^2$
$\text{K}_\text{L}^\text{miss}$ M	$0.83E < \vert\vec{p}\vert < 0.94E$ $\vert\vec{p}\vert > -E + 1625\text{MeV}/c^2$ $\vert\vec{p}\vert < -E + 1825\text{MeV}/c^2$
$\text{K}_\text{L}^\text{miss}$ N	$0.84E < \vert\vec{p}\vert < 0.93E$ $\vert\vec{p}\vert > -E + 1650\text{MeV}/c^2$ $\vert\vec{p}\vert < -E + 1800\text{MeV}/c^2$

Table 5.1: Regions for different kinematical cut in the $\vec{p}$ versus E plane refering to figure 5.2.

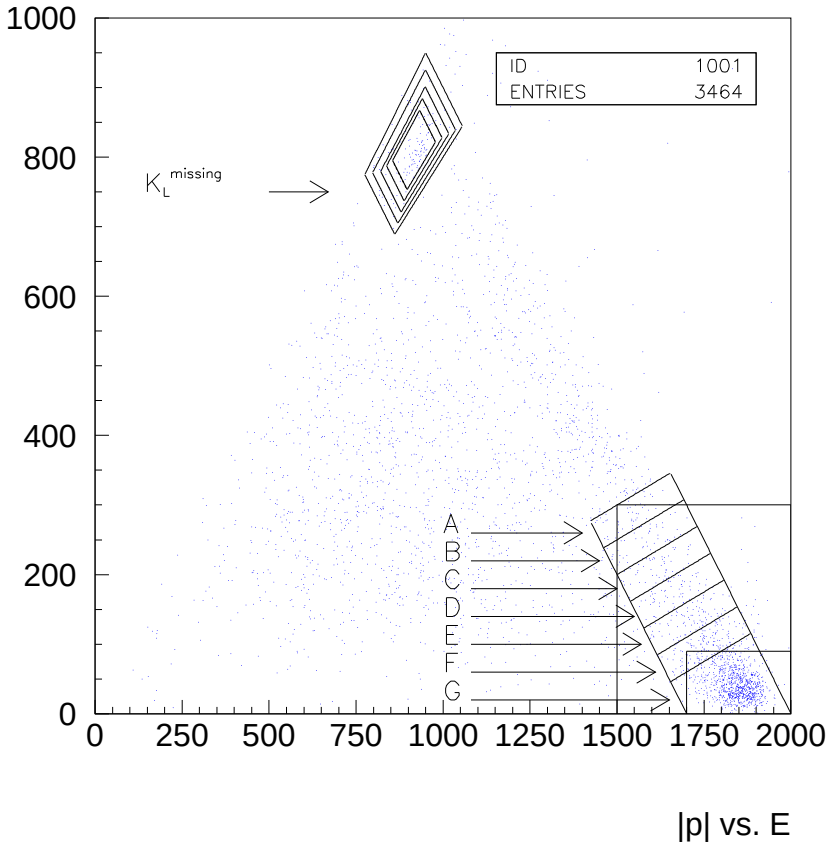

Figure 5.2: $|\vec{p}|$ vs. E. The kinematics for the marked areas are given in table 5.1.

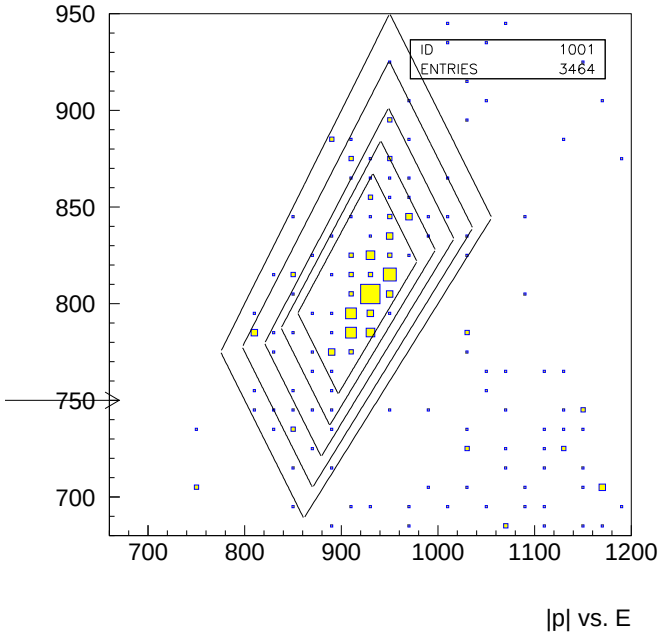

Figure 5.3: $|\vec{p}|$ vs. E. The same as in figure 5.2, but only the K_L-region is shown.

5.1 $\bar{p}p \to \pi^0\pi^0$ and $\pi^0\eta$

The influences of the kinematic cuts and different methods mentioned in section 5 are studied now for several 4-γ final states. Figure 5.4 shows the momentum distribution for π^0's. On the right side a large peak containing $\pi^0\pi^0$ events shows up, the lower momentum is background enhancement.

This background is eliminated due to a cut in the $|\vec{p}|$ vs. E plot. This is illustrated in figure 5.5 for $\pi^0\pi^0$.

First the cuts A to G from table 5.1 are discussed. Region A contains events with missing momentum and up to region G the number of events with missing momentum is decreased.

The same procedure is done for $\pi^0\eta$ (figures 5.4 to 5.6) final state.

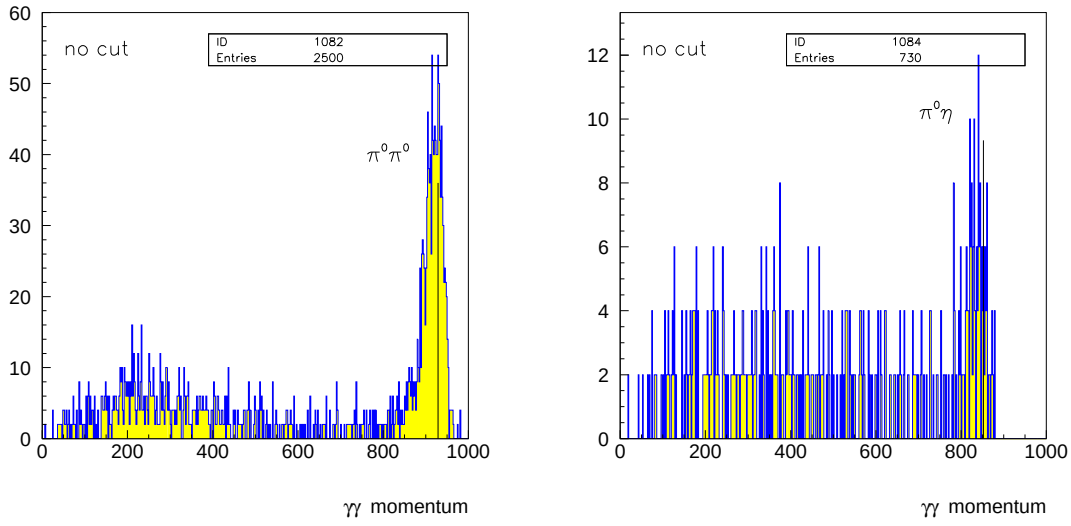

Figure 5.4: (right) Momentum of γ's for $\pi^0\pi^0$ final state. Each event complying with (5.2) causes exactly two entries in the plot due to (5.3).
(left) Momentum of π^0's and η's for $\pi^0\eta$ final state.

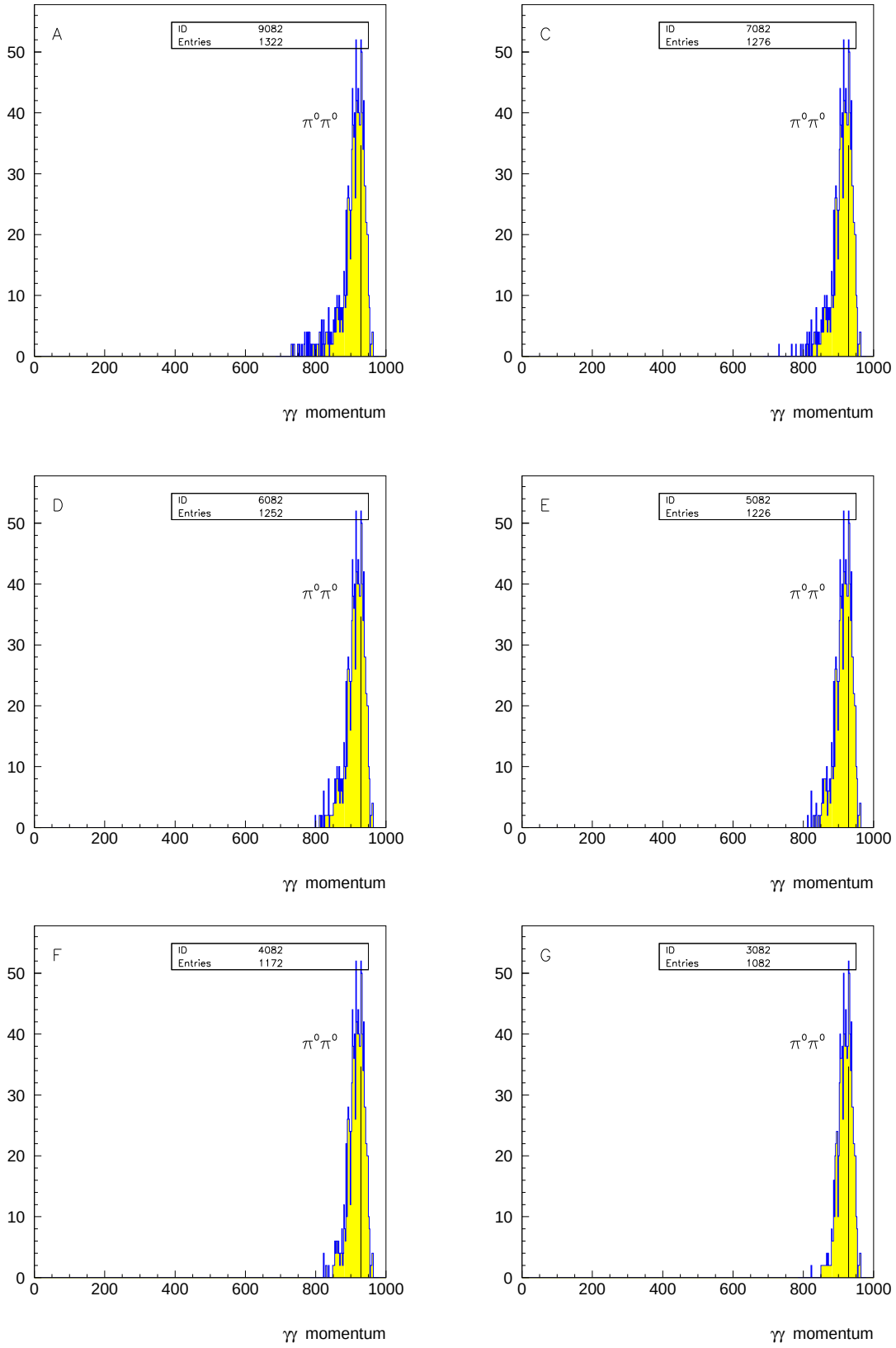

Figure 5.5: Momentum of π^0's for $\pi^0\pi^0$ final state. The letters are refering to the kinematical regions listed in table 5.1. Each event complying with (5.2) causes exactly two entries in the plot due to (5.3).

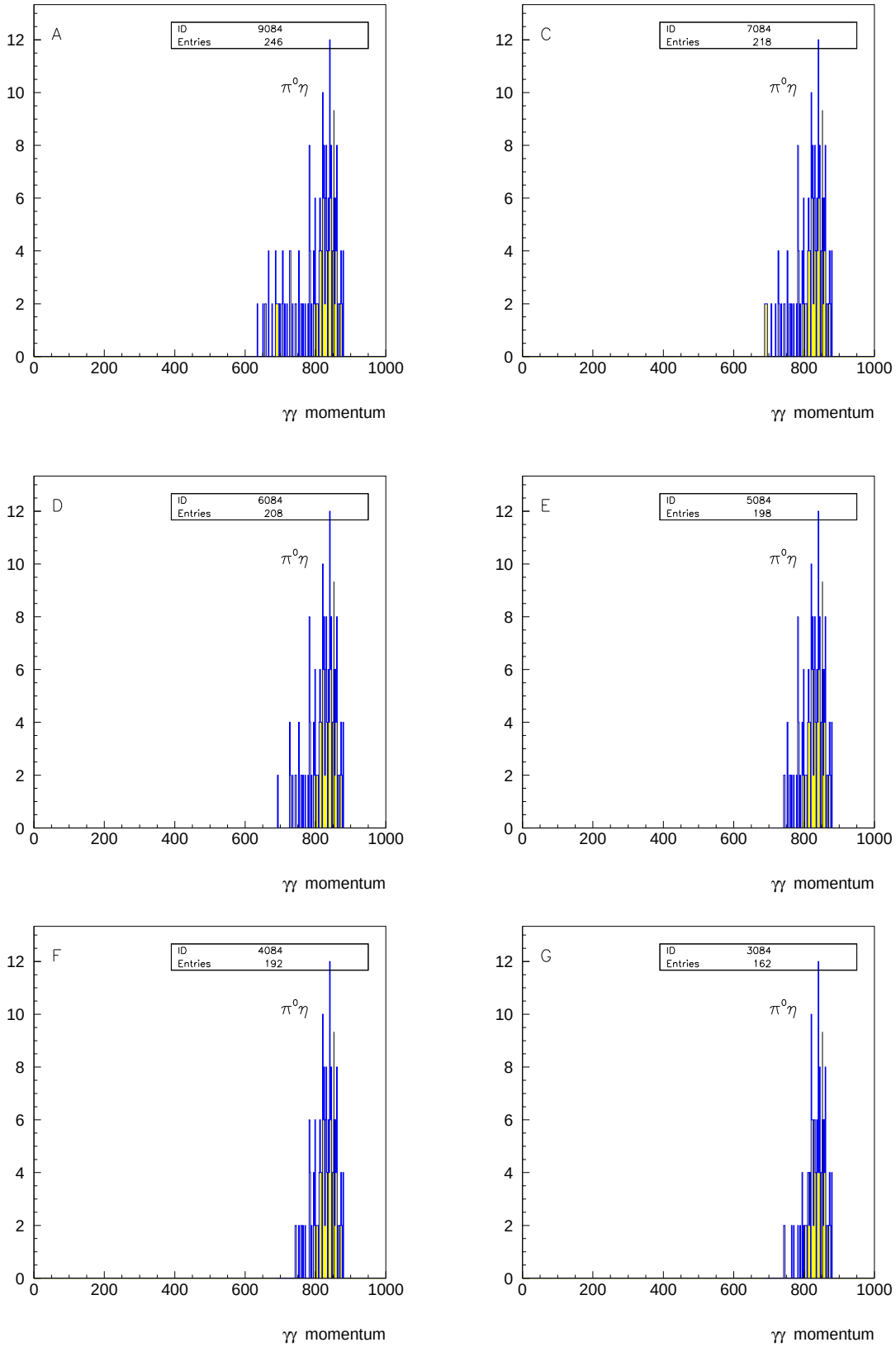

Figure 5.6: Momentum of π^0's and η's for $\pi^0\eta$ final state. The letters are refering to the kinematical regions listed in table 5.1. Each event complying with (5.2) causes exactly two entries in the plot due to (5.3).

5.2 $\bar{p}p \to K_L K_S$

All $\bar{p}p \to K_L K_S$ events ($K_S \to \pi^0\pi^0$, K_L is not detected) can be found in the regions J to N (figure 5.2). The corresponding momentum distribution of the four γ's is shown in figure 5.7 (left) and the missing mass distribution in figure 5.7 (right).

The K_L-interaction probability:

To make sure that the K_L was not lost in the hole around the beam pipe it is asked for a measured momentum within $21° < \theta < 159°$. This ensures that the missing momentum of the non-interacting K_L points to a sensitive detector region. The probability that the K_L does not interact in the crystals is $(42.8 \pm 2.7)\%$ [7]. This value was derived for $|\vec{p}(K_L)| = 795\,\mathrm{MeV}/c$, which is the momentum of interest.

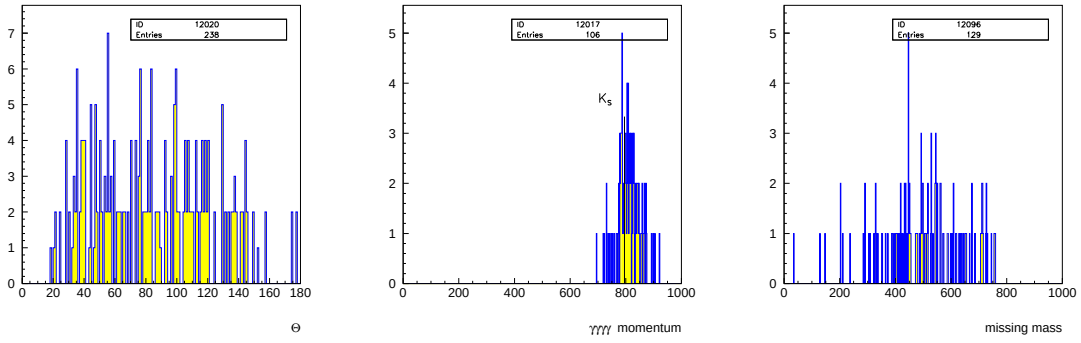

Figure 5.7: (left) Angular distribution for the measured momentum.
(center) Momentum of four γ's for $K_L K_S$ final state ($21° < \theta < 159°$). Each event complying with (5.2) causes exactly one entry in the plot.
(right) Missing mass of four γ's for $K_L K_S$ final state.
Each event complying with (5.2) causes exactly one entry in the plots for region J (table 5.1).

5.3 $\pi^0\pi^0$ Monte Carlo events

The π^0 was produced with its measured decay ratio into 2γ's of 98.802%. Therefore no further corrections are needed.

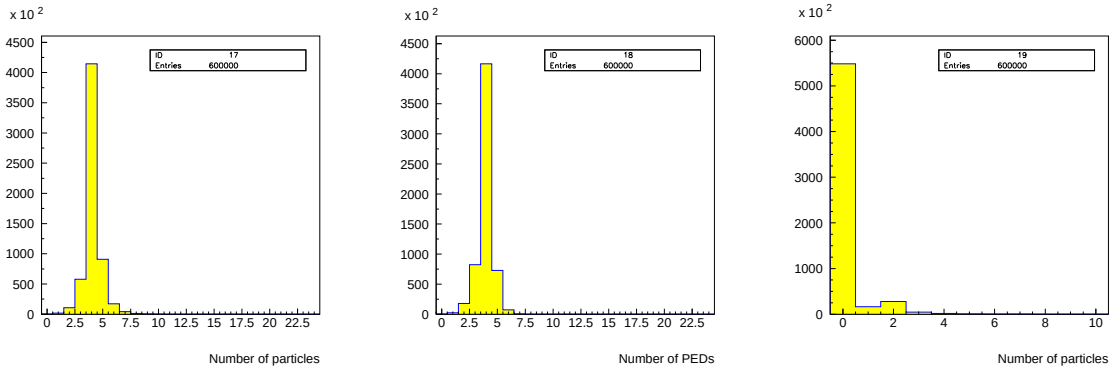

Figure 5.8: The number of particles, PEDs and charged tracks for 600 000 produced Monte Carlo events.

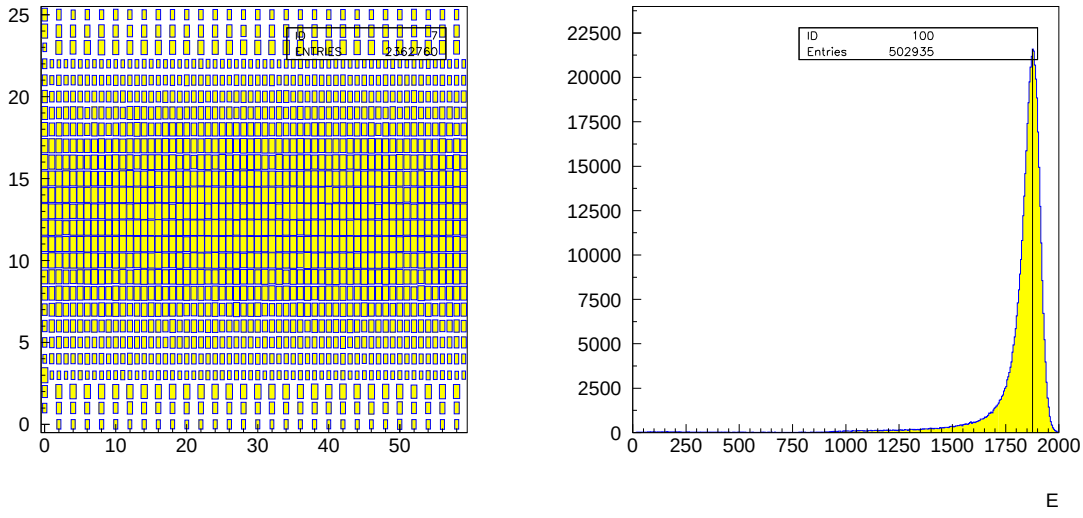

Figure 5.9: (left) Unfolded view of the calorimeter for Monte Carlo events.
(right) Energy of all γ's for Monte Carlo events.

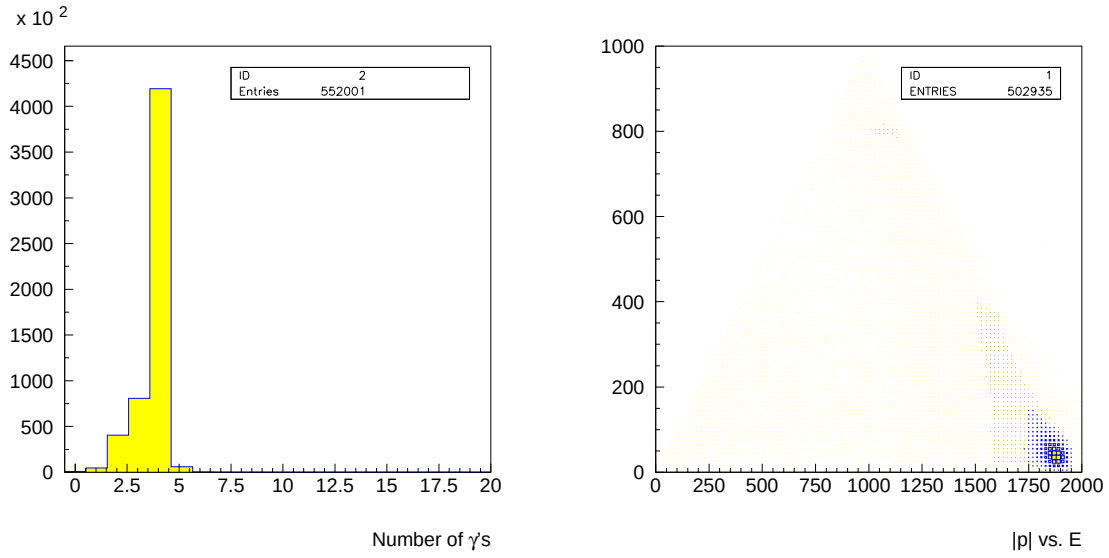

Figure 5.10: (left) γ distribution for Monte Carlo events (419 313 4-γ events).
(right) $|\vec{p}|$ vs. E for Monte Carlo events.

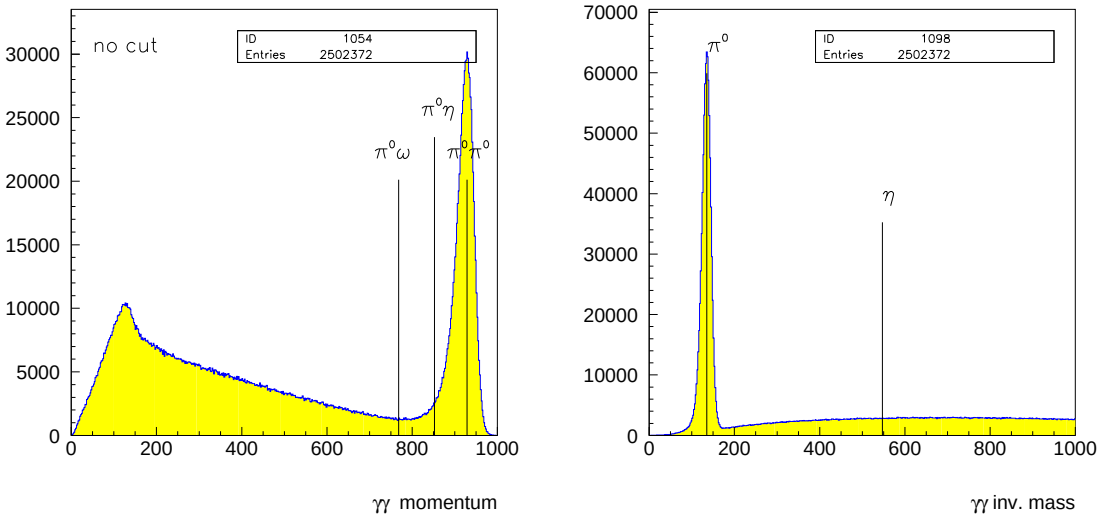

Figure 5.11: (left) Momentum of all 2 π^0's. Each $\pi^0\pi^0$ events causes two entries in the peak on the right side.
(right) Invariant masses of 2 γ's.

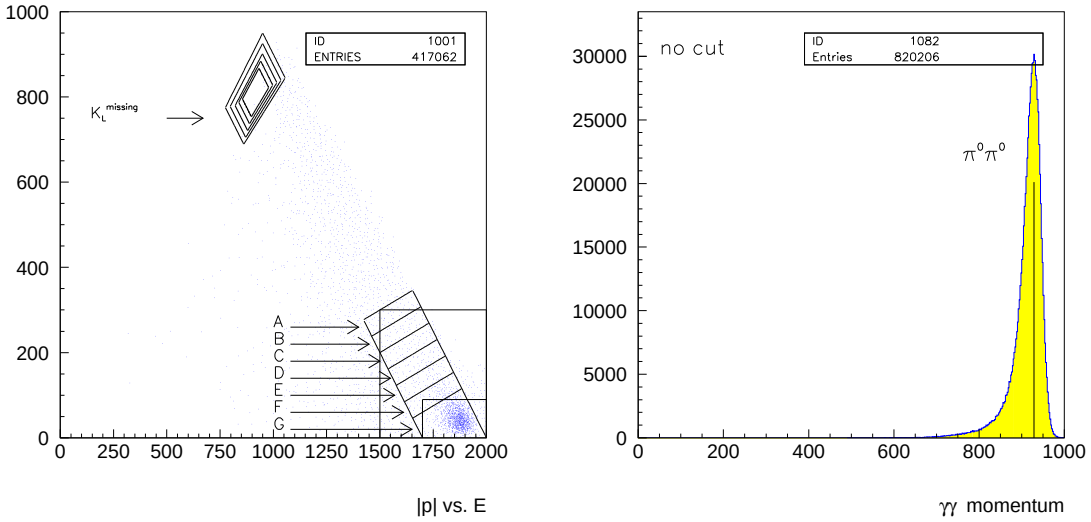

Figure 5.12: (left) $|\vec{p}|$ vs. E. The kinematics for the marked areas are given in table 5.1.
(right) Momentum of π^0's for $\pi^0\pi^0$ final state.
Each event complying with (5.2) causes exactly two entries in the plot due to (5.3).

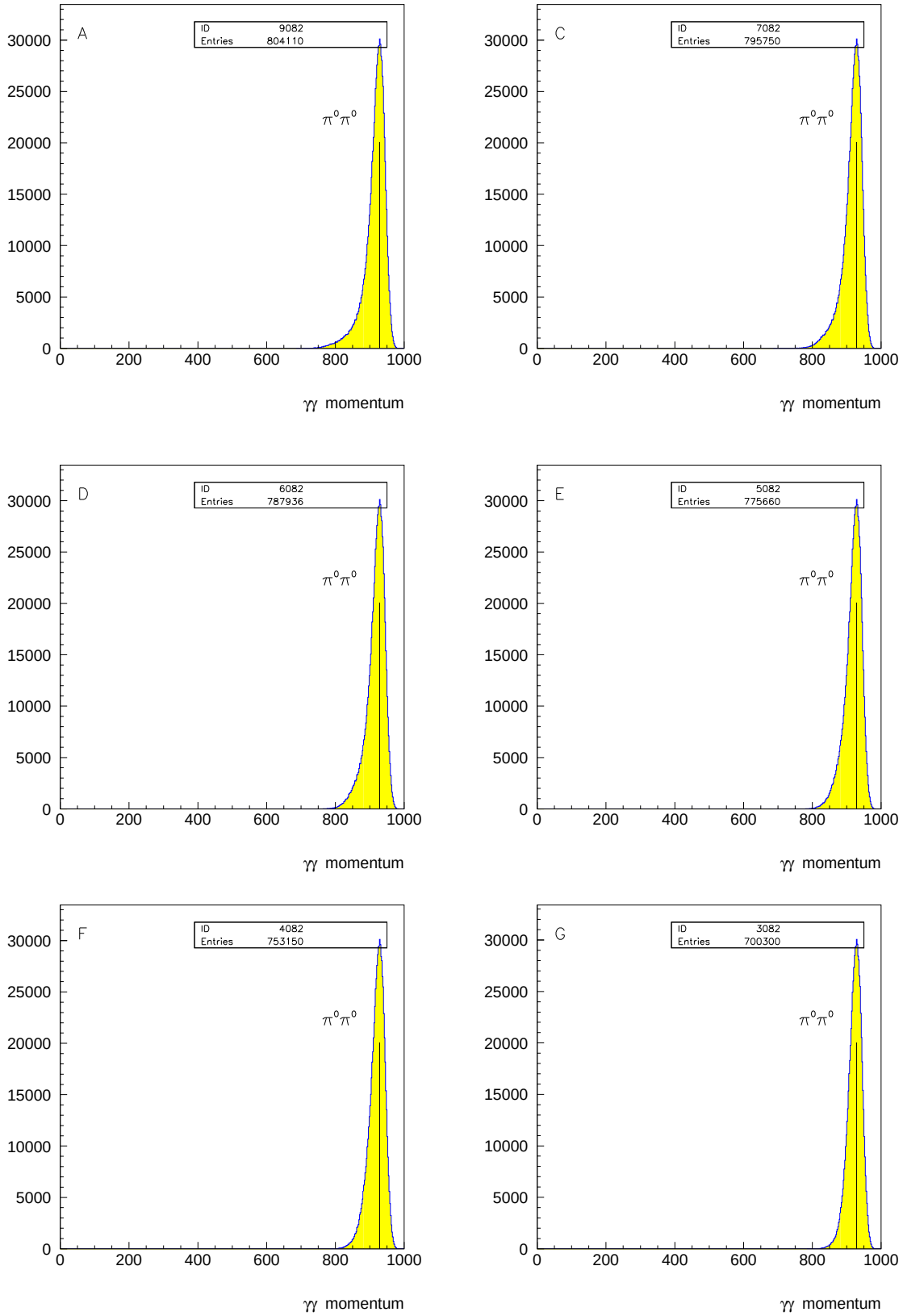

Figure 5.13: Momentum of π^0's for $\pi^0\pi^0$ final state. The letters are refering to the kinematical regions listed in table 5.1.
Each event complying with (5.2) causes exactly two entries in the plot due to (5.3).

5.4 $\pi^0\eta$ Monte Carlo events

η's decaying with 100% into 2γ have been produced. Therefore one has to correct the value with $(39.25 \pm 0.31)\%$ [9].

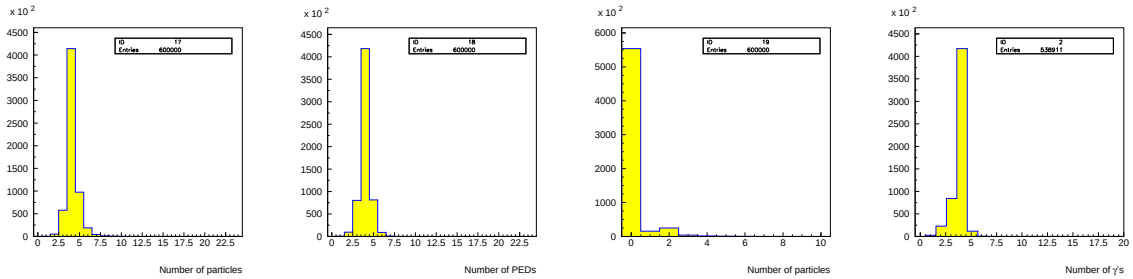

Figure 5.14: The number of particles, PEDs and charged tracks for 600 000 produced Monte Carlo events. γ distribution for Monte Carlo events.

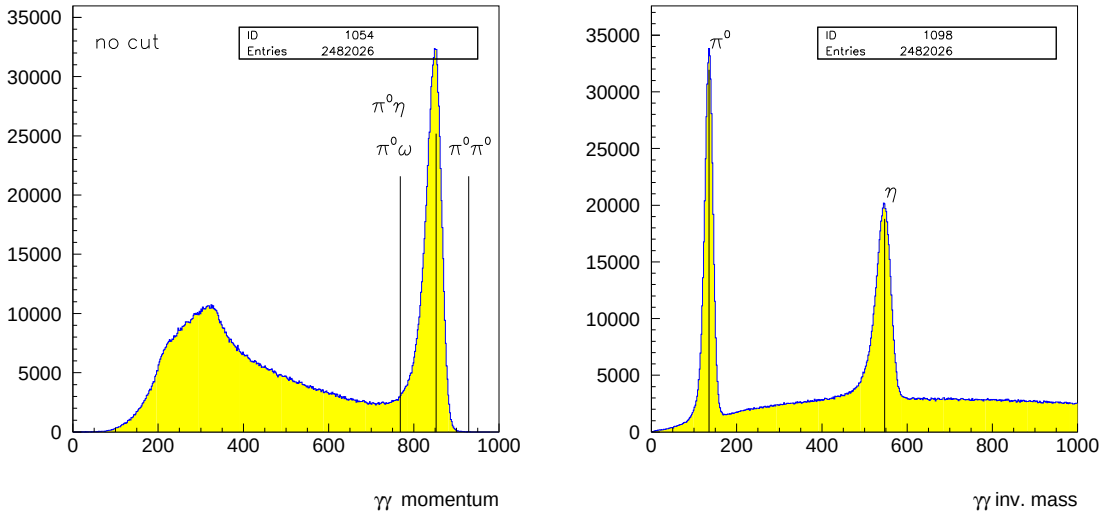

Figure 5.15: (left) Momentum of π^0's. Each $\pi^0\eta$ events causes two entries in the peak on the right side.
(right) Invariant masses of 2 γ's.

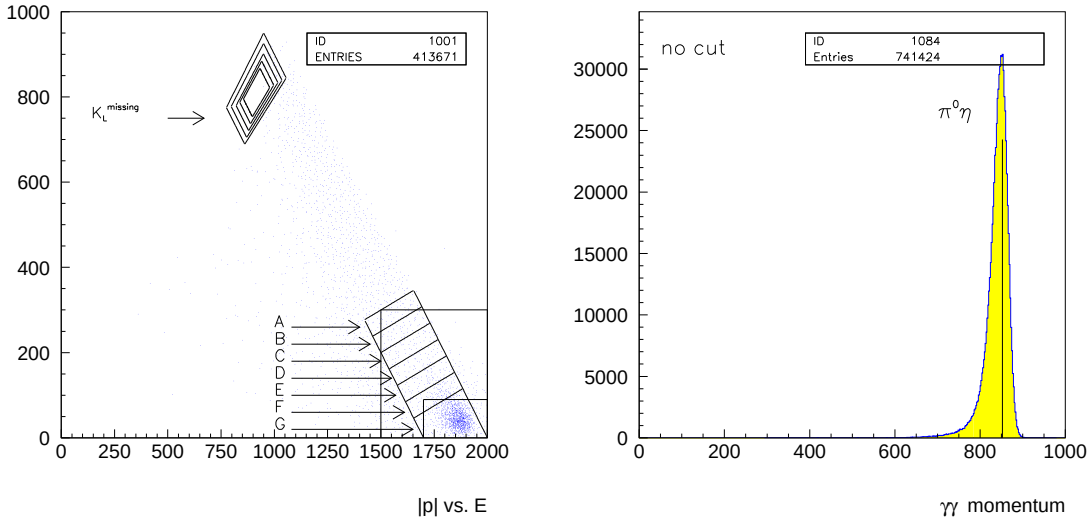

Figure 5.16: (left) $|\vec{p}|$ vs. E. The kinematics for the marked areas are given in table 5.1. (right) Momentum of γ's for $\pi^0\eta$ final state. Each event complying with (5.2) causes exactly two entries in the plot due to (5.3).

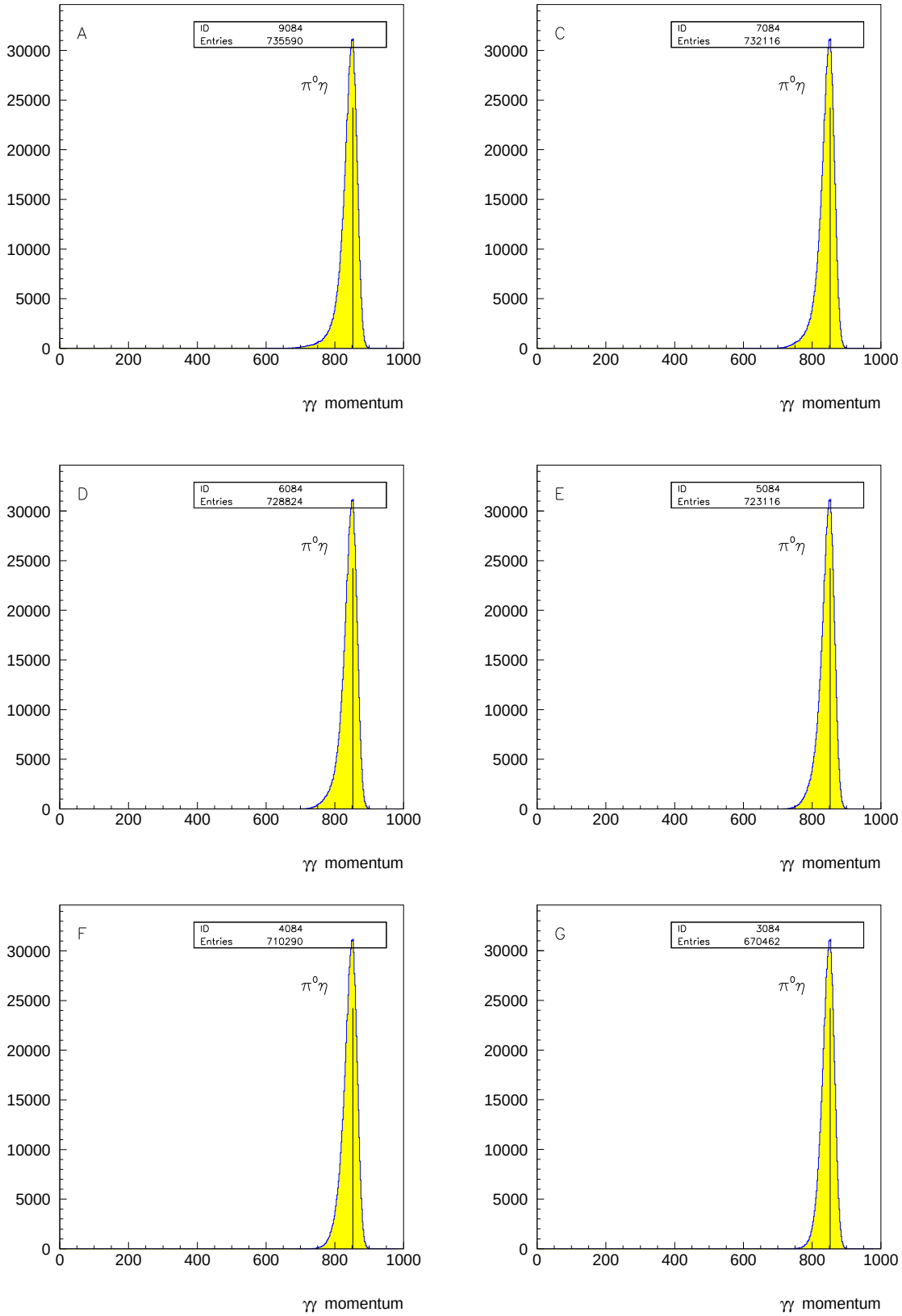

Figure 5.17: Momentum of π^0's and η's for $\pi^0\eta$ final state. The letters are refering to the kinematical regions listed in table 5.1. Each event complying with (5.2) causes exactly two entries in the plot due to (5.3).

5.5 $K_S K_L$ Monte Carlo events

The produced K_S's decay with 100% into $\pi^0\pi^0$. The K_L decays into two non-interacting Monte Carlo particles, called geantinos. The very short decay time of $\tau = 10^{-20}$ sec ensures that there is no interaction between the K_L and the detector possible.

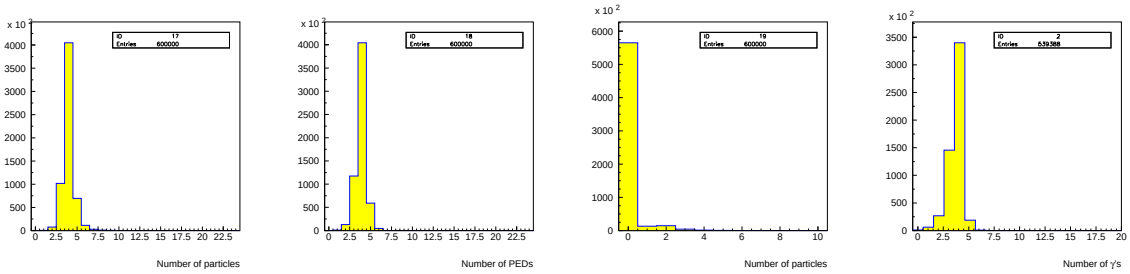

Figure 5.18: The number of particles, PEDs and charged tracks for 600 000 produced Monte Carlo events. γ distribution for Monte Carlo events.

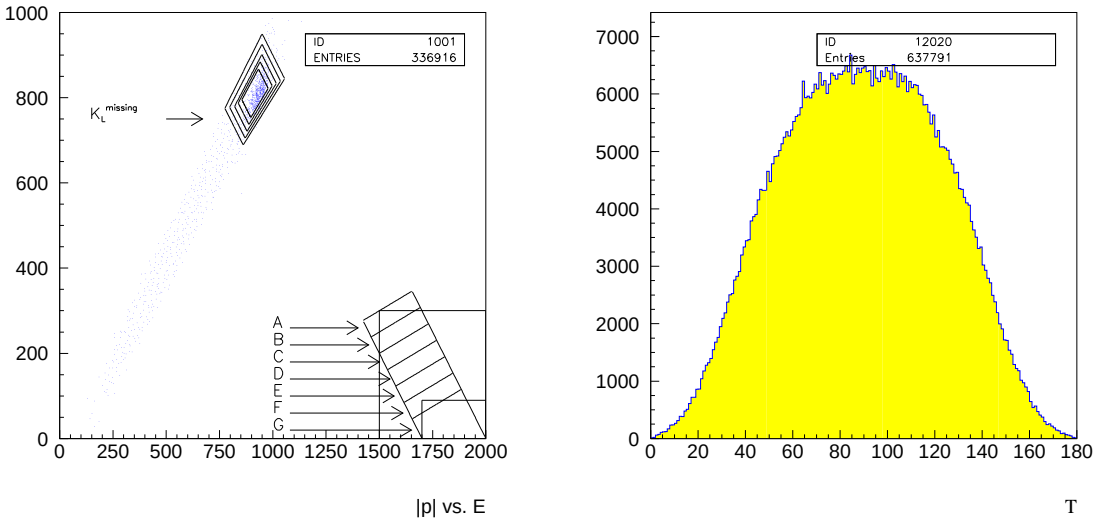

Figure 5.19: (left) $|\vec{p}|$ vs. E for Monte Carlo events.
(right) Angular distribution for measured momentum.

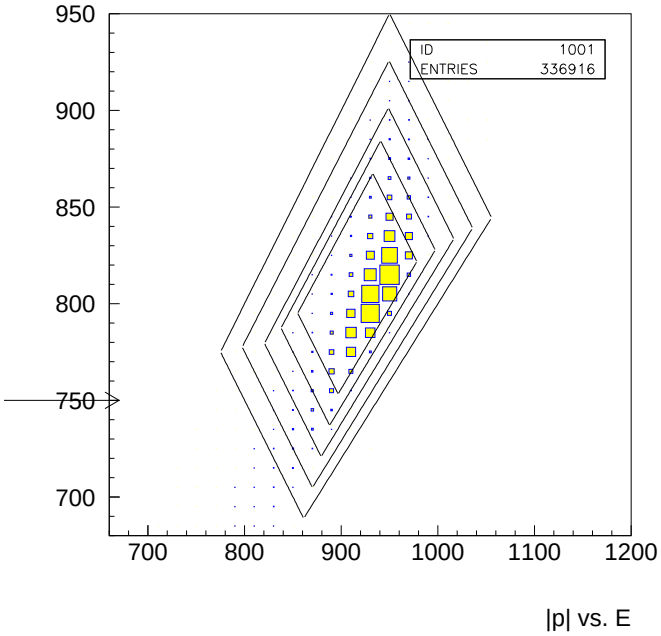

Figure 5.20: The same as in figure 5.19, but only the K_L-region is shown.

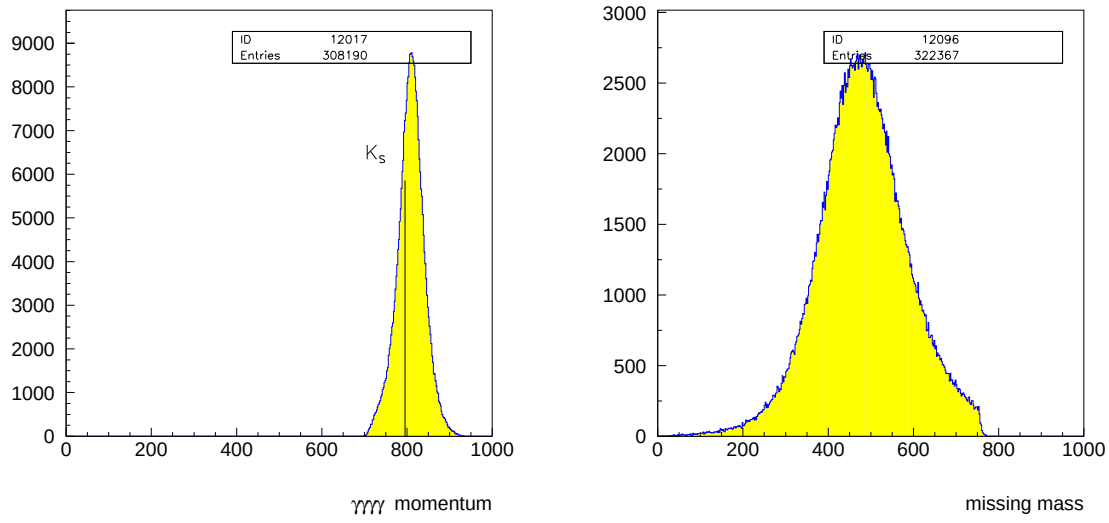

Figure 5.21: (left) Momentum of 2 γ's for $K_L K_S$ final state ($21° < \theta < 159°$).
(right) Missing mass of four γ's for $K_L K_S$ final state.
Each event complying with (5.2) causes exactly one entry in the plot.

5.6 $\omega\pi^0$ Monte Carlo events

From a previous analysis it is known that the branching ratio for $\bar{p}p \rightarrow \omega\pi^0$ is about 10 times larger than for $\pi^0\pi^0$ ($(5.73 \pm 0.47) \cdot 10^{-3}$) [2]). The ω decays into $\pi^0\gamma$ with a ratio of $(8.5 \pm 0.5)\%$ [9]. Events with a lost γ from ω decay may fake a π^0. To investigate this $\omega\pi^0$ Monte Carlo events have been produced with the ω decaying into $\pi^0\gamma$.

Histograms 5.22 show the produced $\pi^0\omega$ events. In the spectra of the 3γ and 2γ invariant masses clear peaks for the ω and π^0 show up over a combinatorical background (30 entries for each event).

The histograms 5.24 to 5.27 illustrate the reconstruction for the $\pi^0\pi^0$ final state.

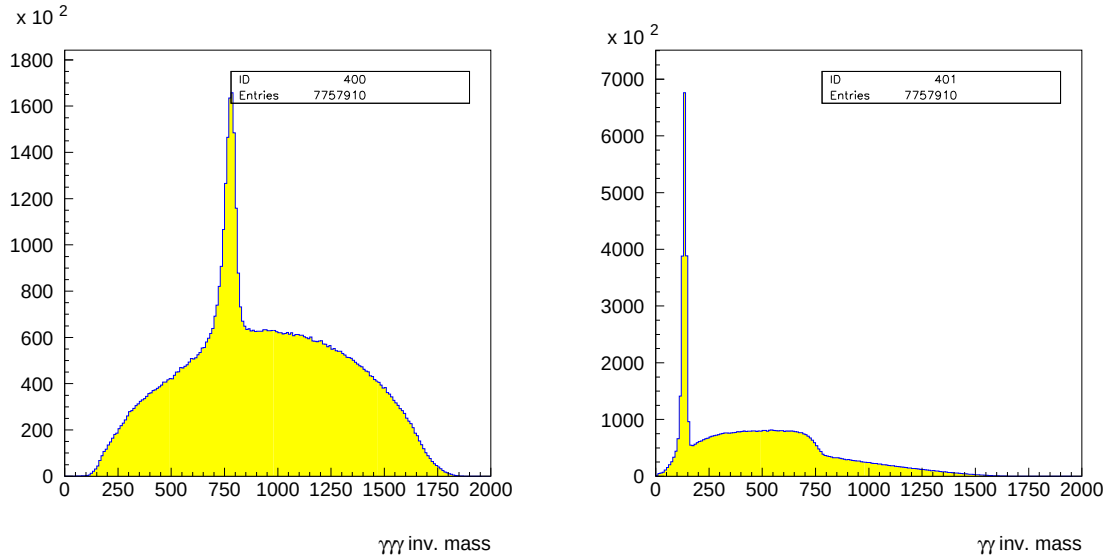

Figure 5.22: (left) invariant $\gamma\gamma\gamma$ mass(right) invariant $\gamma\gamma$ mass

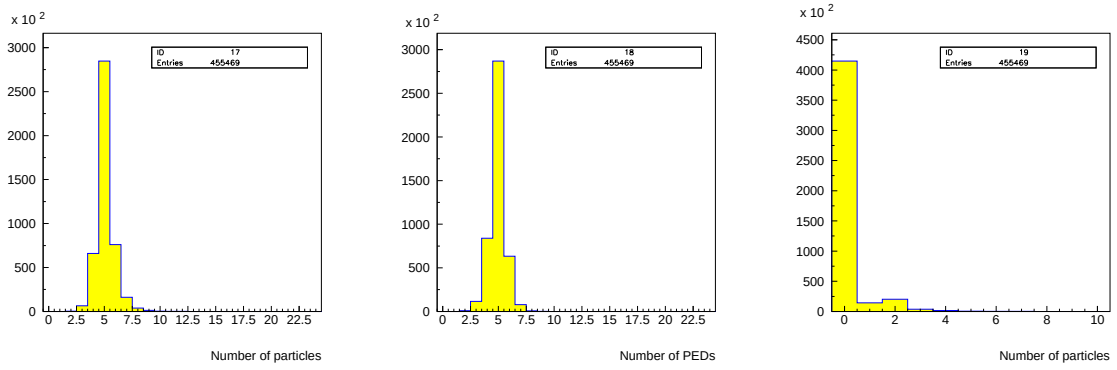

Figure 5.23: The number of particles, PEDs and charged tracks for 455 469 produced Monte Carlo events.

Now the number of $\omega\pi^0$ events wrongly assigned to the reconstructed $\pi^0\pi^0$ data set can be estimated, see figure 5.13 (for notation see section 5.7).

$$\#\text{fake events} = \#(\text{analysed events}) \cdot (\text{vertex correction}) \cdot \text{BR}(\bar{\text{p}}\text{p} \to \omega\pi^0) \cdot \text{BR}(\omega \to \pi^0\gamma) \cdot \frac{\#(\text{as } \pi^0\pi^0 \text{ reconstructed} \omega\pi^0 \text{ MC events})}{\#(\text{produced } \omega\pi^0 \text{ MC events})} \tag{5.4}$$

Compared with the values listed in table 5.3 the number of $\omega\pi^0$ background events is negligible.

region	#(rec. MC)	#fake events
A	2 859	4.685 ± 0.454
B	2 363	3.872 ± 0.375
C	1 841	3.017 ± 0.292
D	1 342	2.199 ± 0.213
E	1 024	1.678 ± 0.163
F	897	1.470 ± 0.142
G	789	1.293 ± 0.125

Table 5.2: Fake $\omega\pi^0$ events. The kinematical region refers to table 5.1.

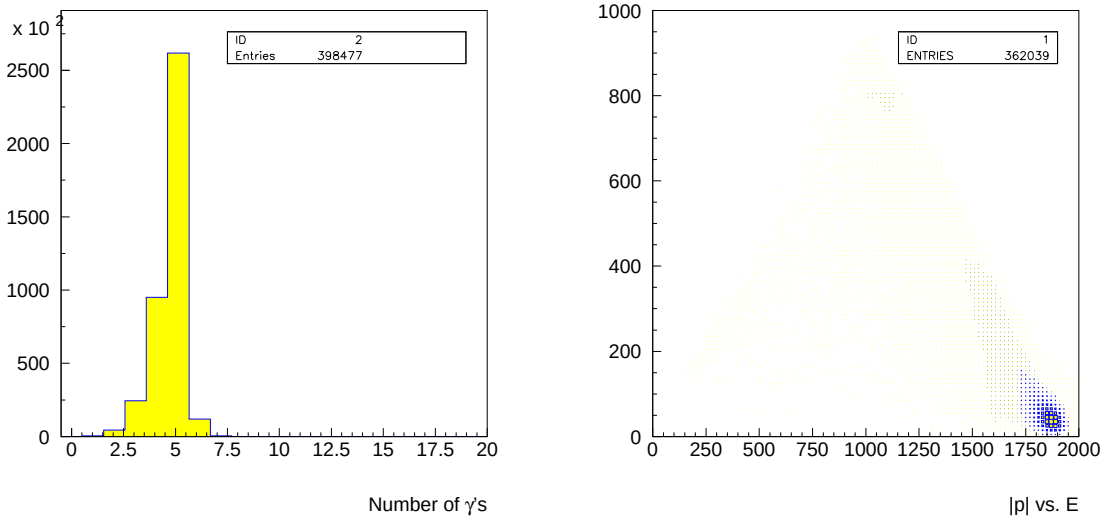

Figure 5.24: (left) γ distribution for Monte Carlo events (261 776 5-γ events). (right) $|\vec{p}|$ vs. E for Monte Carlo events.

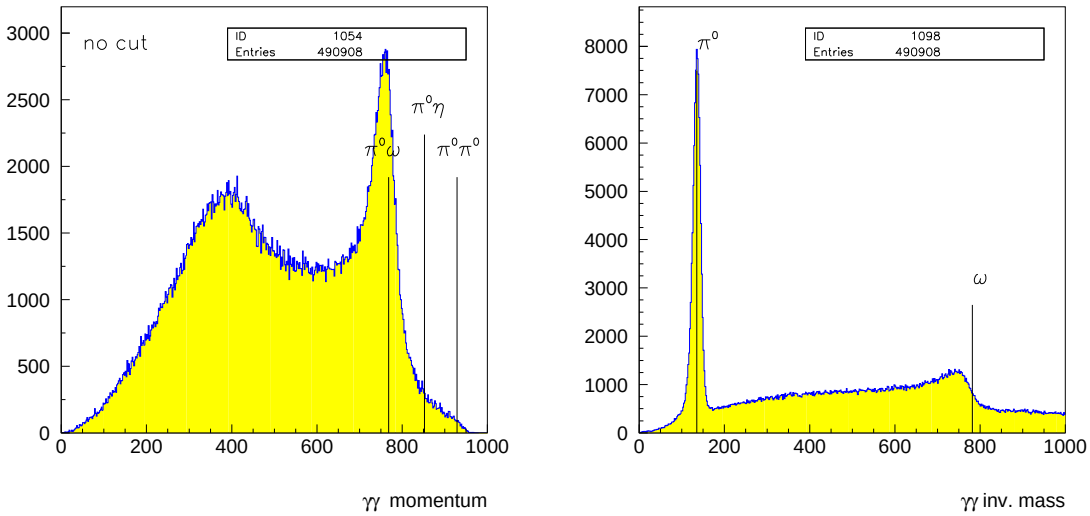

Figure 5.25: (left) Momentum of all 2 π^0's. Each $\pi^0\pi^0$ events causes two entries in the peak on the right side.
(right) Invariant masses of 2 γ's.

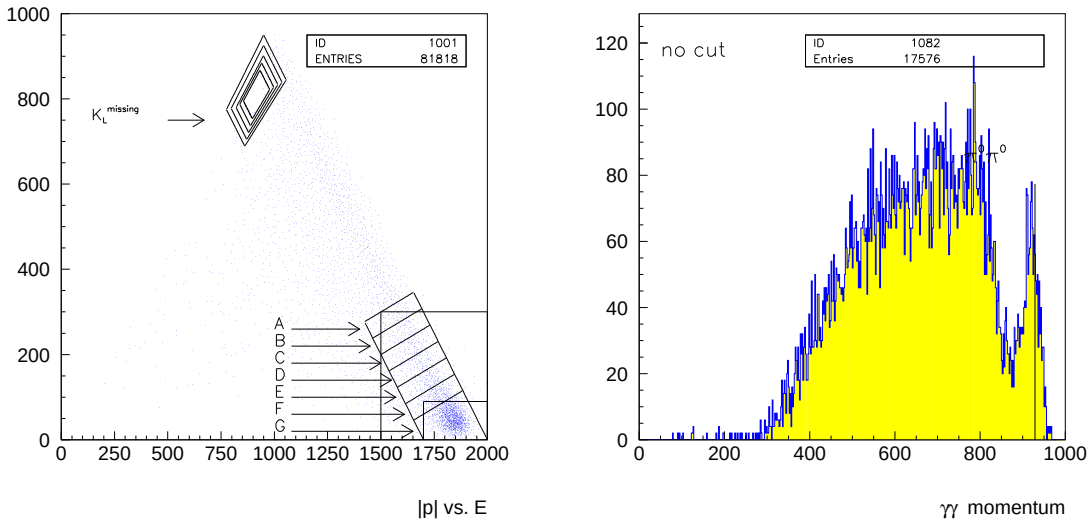

Figure 5.26: (left) $|\vec{p}|$ vs. E. The kinematics for the marked areas are given in table 5.1.
(right) Momentum of π^0's for $\pi^0\pi^0$ final state.
Each event complying with (5.2) causes exactly two entries in the plot due to (5.3).

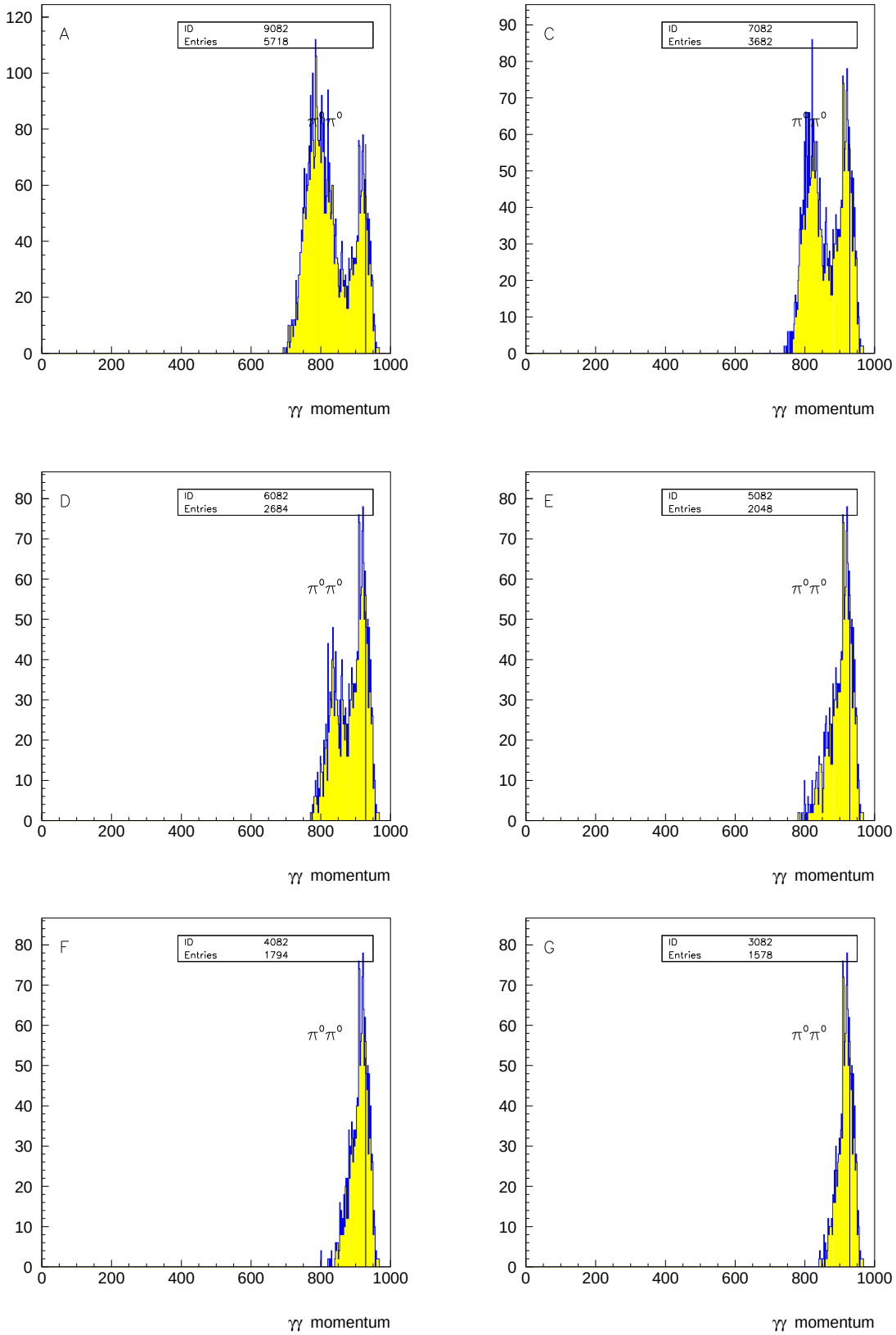

Figure 5.27: Momentum of π^0's for $\pi^0\pi^0$ final state. The letters are refering to the kinematical regions listed in table 5.1.
Each event complying with (5.2) causes exactly two entries in the plot due to (5.3).

5.7 The Branching Ratios

The formula to derive a value for the branching ratio is introduced and the results will be discussed:

$$BR(\bar{\mathrm{p}}\mathrm{p} \to \mathrm{xx}) = \frac{\dfrac{\#(xx)}{\#(\text{analysed events}) \cdot (\text{vertex correction})}}{\dfrac{\#(\text{reconstructed MC events})}{\#(\text{produced MC events})}} \tag{5.5}$$

First the all neutral branching ratios. Due to the fact that the Monte Carlo π^0 decays into 2γ with 98.802% the branching ratio for $\pi^0\pi^0$ is calculated following (5.5). On the other hand the CBGEANT η decays only into 2γ. So the peak entry for the Monte Carlo events must be multiplied by a factor 0.3925 for each η (MC correction).

region	$\#(\pi^0\pi^0)$	#(rec. MC)	$BR(\bar{\mathrm{p}}\mathrm{p} \to \pi^0\pi^0)$
A	661	402 055	$(6.437 \pm 0.410) \cdot 10^{-4}$
B	651	400 334	$(6.367 \pm 0.407) \cdot 10^{-4}$
C	638	397 875	$(6.278 \pm 0.403) \cdot 10^{-4}$
D	626	393 968	$(6.221 \pm 0.401) \cdot 10^{-4}$
E	613	387 830	$(6.188 \pm 0.400) \cdot 10^{-4}$
F	586	376 575	$(6.092 \pm 0.398) \cdot 10^{-4}$
G	541	350 150	$(6.049 \pm 0.401) \cdot 10^{-4}$
H	684	405 360	$(6.606 \pm 0.419) \cdot 10^{-4}$
I	539	347 255	$(6.077 \pm 0.403) \cdot 10^{-4}$

Table 5.3: $\pi^0\pi^0$ branching ratios. The kinematical region refers to table 5.1.

region	$\#(\pi^0\eta)$	#(rec. MC)	$BR(\bar{\mathrm{p}}\mathrm{p} \to \pi^0\eta)$
A	123	367 795	$(3.336 \pm 0.345) \cdot 10^{-4}$
B	117	367 080	$(3.179 \pm 0.335) \cdot 10^{-4}$
C	109	366 058	$(2.970 \pm 0.322) \cdot 10^{-4}$
D	104	364 412	$(2.847 \pm 0.314) \cdot 10^{-4}$
E	99	361 558	$(2.731 \pm 0.307) \cdot 10^{-4}$
F	96	355 145	$(2.696 \pm 0.307) \cdot 10^{-4}$
G	81	335 231	$(2.410 \pm 0.294) \cdot 10^{-4}$
H	124	369 055	$(3.351 \pm 0.345) \cdot 10^{-4}$
I	82	332 716	$(2.458 \pm 0.299) \cdot 10^{-4}$

Table 5.4: $\pi^0\eta$ branching ratios. The kinematical region refers to table 5.1.

The determination of the $\mathrm{K_L K_S}$ branching ratio requires more modifications of (5.5). On one hand only $(31.39 \pm 0.28)\%$ of the $\mathrm{K_S}$ decay into $\pi^0\pi^0$ and on the other hand only non-interacting $\mathrm{K_L}$'s are detected. Therefore the number of reconstructed $\mathrm{K_L K_S}$ must be multiplied by a factor of $0.3139 \cdot 0.428$ (see section 5.2).

region	#($K_L K_S$)	#(rec. MC)	$BR(\bar{p}p \to K_L K_S)$
J	106	308 190	$(1.002 \pm 1.097) \cdot 10^{-3}$
K	101	304 549	$(9.664 \pm 1.079) \cdot 10^{-4}$
L	88	296 844	$(8.639 \pm 1.019) \cdot 10^{-4}$
M	84	280 223	$(8.735 \pm 1.050) \cdot 10^{-4}$
N	69	239 995	$(8.378 \pm 1.094) \cdot 10^{-4}$

Table 5.5: $K_L K_S$ neutral branching ratios. The kinematical region refers to table 5.1.

The different values given in the tables above are used to calculate the final value and the error. The correction of $(3.7 \pm 0.7)\%$ for annihilations outside the vertex and the Monte Carlo uncertainty is 5%.

Figure 5.2 shows that the kinematical regions E and F are the best cuts for the $\pi^0\pi^0$ and $\pi^0\eta$ branching ratio.

A comparison between figures 5.3 and 5.20 shows that it makes sense to use the region L for the determination of the $K_L K_S$ branching ratio.

$$BR(\bar{p}p(LH_2) \to \pi^0\pi^0) = (6.14 \pm 0.40) \cdot 10^{-4} \tag{5.6}$$

$$BR(\bar{p}p(LH_2) \to \pi^0\eta) = (2.71 \pm 0.30) \cdot 10^{-4} \tag{5.7}$$

$$BR(\bar{p}p(LH_2) \to K_L K_S) = (8.64 \pm 1.02) \cdot 10^{-4} \tag{5.8}$$

Chapter 6

2-prong events

From all events remaining after the preselection 2-prong events are selected.

Definition for a 2-prong event:

- number of hits per track ≥ 15
- normal convergence for track reconstruction
- first layer $1-3$, last layer $20-23$

Figure 6.1 shows the momenta of the two prongs from the April 1996 run (LH_2).

The $|\vec{p}|$ versus E distribution in figure 6.2 illustrates the kinematical regions for different event types. There are three interesting regions. The fully reconstructed $\pi^+\pi^-$ final states are located in boxes G to L. Due to the fact that it is unknown whether a charged particle is a pion or a kaon, the energy for kaons is to low. So they are located in regions A to F. For the $K_S K_L^{miss}$ final state the whole momentum and energy of the K_L are missing. Unfortunately it is not possible to determine a branching ratio for this channel. The background in this region is very strong and no significant structure is visible.

Furthermore, the event topology of a two-body final state must be compatible with two back-to-back (collinear) charged tracks. This requires an angle between the two tracks of 180°. Figure 6.3 shows the distribution. This is true for all events in regions A to L.

6.1 $\bar{p}p \to \pi^+\pi^-$ and K^+K^-

First the collinear events in regions A and L have been investigated. Figure 6.1 shows the momentum distribution of the two charged particles. Two peaks for K^+K^- and $\pi^+\pi^-$ collinear two-body events show up. On the left side there is a large background.

Now the kinematics in regions A to F for K^+K^- events and G to L for $\pi^+\pi^-$ events are separated. Figure 6.4 and 6.8 illustrate examples for the momentum distributions of the charged tracks.

A	$\lvert\vec{p}\rvert < 150\,\mathrm{MeV}/c$ $1500\,\mathrm{MeV}/c^2 < E < 1700\,\mathrm{MeV}/c^2$
B	$\lvert\vec{p}\rvert < 120\,\mathrm{MeV}/c$ $1500\,\mathrm{MeV}/c^2 < E < 1700\,\mathrm{MeV}/c^2$
C	$\lvert\vec{p}\rvert < 90\,\mathrm{MeV}/c$ $1500\,\mathrm{MeV}/c^2 < E < 1700\,\mathrm{MeV}/c^2$
D	$\lvert\vec{p}\rvert < 150\,\mathrm{MeV}/c$ $1500\,\mathrm{MeV}/c^2 < E < 1740\,\mathrm{MeV}/c^2$
E	$\lvert\vec{p}\rvert < 120\,\mathrm{MeV}/c$ $1500\,\mathrm{MeV}/c^2 < E < 1740\,\mathrm{MeV}/c^2$
F	$\lvert\vec{p}\rvert < 90\,\mathrm{MeV}/c$ $1500\,\mathrm{MeV}/c^2 < E < 1740\,\mathrm{MeV}/c^2$
G	$\lvert\vec{p}\rvert < 150\,\mathrm{MeV}/c$ $1740\,\mathrm{MeV}/c^2 < E < 1950\,\mathrm{MeV}/c^2$
H	$\lvert\vec{p}\rvert < 120\,\mathrm{MeV}/c$ $1740\,\mathrm{MeV}/c^2 < E < 1950\,\mathrm{MeV}/c^2$
I	$\lvert\vec{p}\rvert < 90\,\mathrm{MeV}/c$ $1740\,\mathrm{MeV}/c^2 < E < 1950\,\mathrm{MeV}/c^2$
J	$\lvert\vec{p}\rvert < 150\,\mathrm{MeV}/c$ $1740\,\mathrm{MeV}/c^2 < E < 2000\,\mathrm{MeV}/c^2$
K	$\lvert\vec{p}\rvert < 120\,\mathrm{MeV}/c$ $1740\,\mathrm{MeV}/c^2 < E < 2000\,\mathrm{MeV}/c^2$
L	$\lvert\vec{p}\rvert < 90\,\mathrm{MeV}/c$ $1740\,\mathrm{MeV}/c^2 < E < 2000\,\mathrm{MeV}/c^2$

Table 6.1: Regions for different kinamatical cut in the $\vec{p}$ versus E plane referring to figure 6.2. (kaons: A to F, pions: G to L)

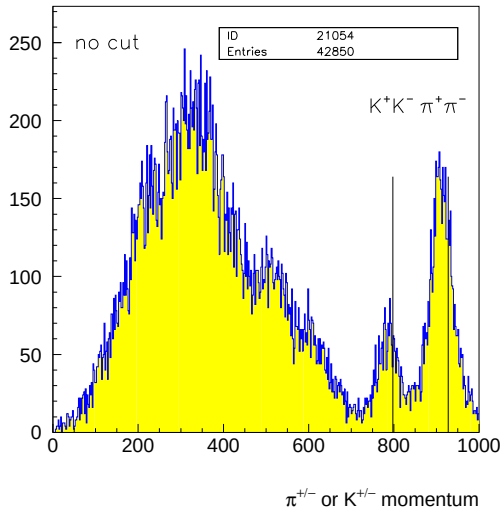

Figure 6.1: Momentum of two prongs. Each event causes one entry.

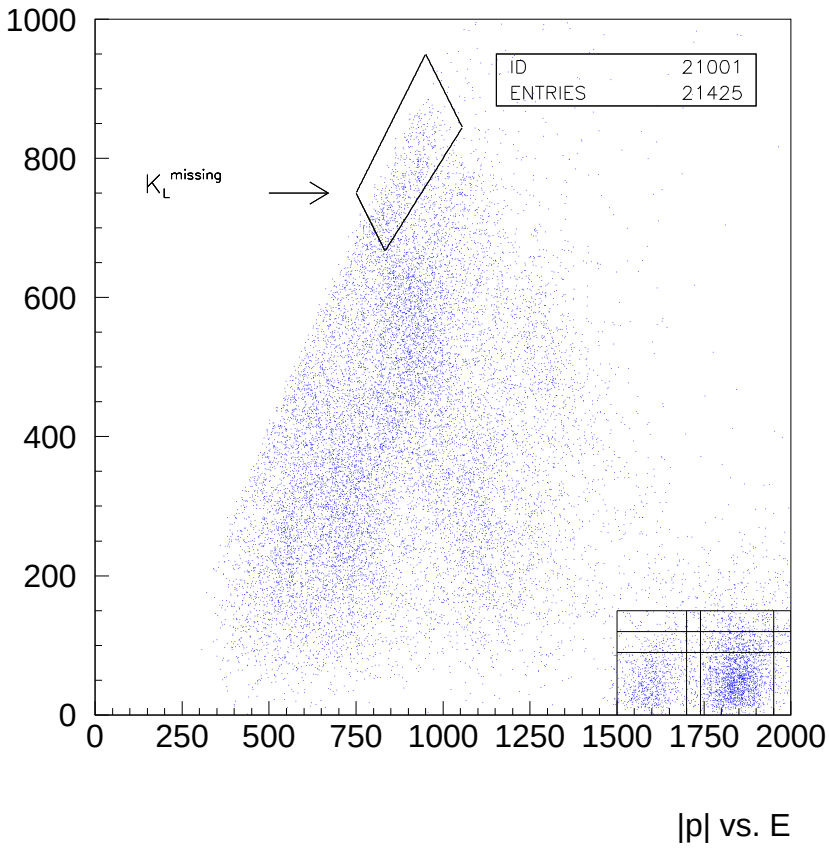

Figure 6.2: $|\vec{p}|$ vs. E for 2-prong data.

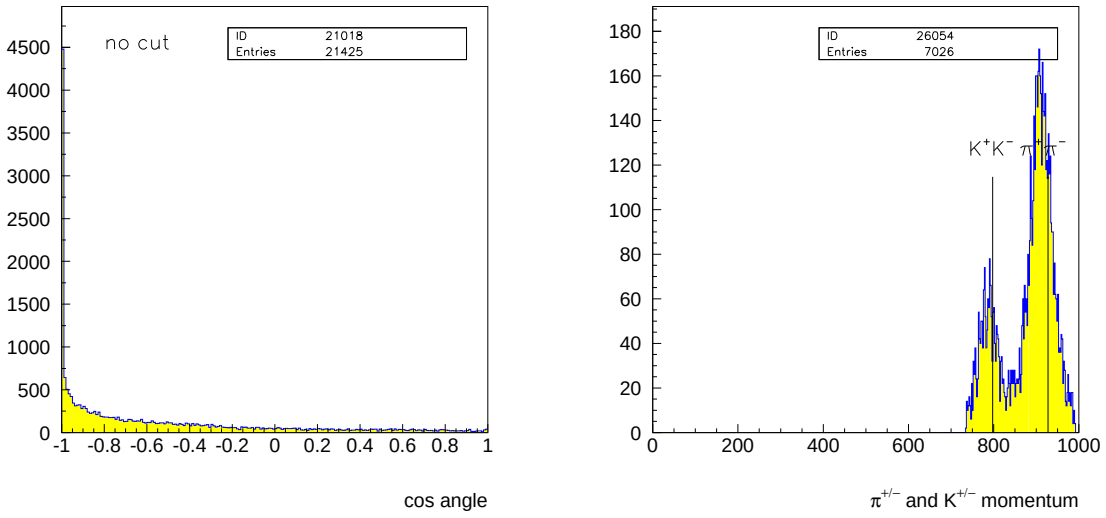

Figure 6.3: (left) cos of the angle between the two tracks.
(right) Momentum of two prongs. Each event causes one entry (regions A and B).

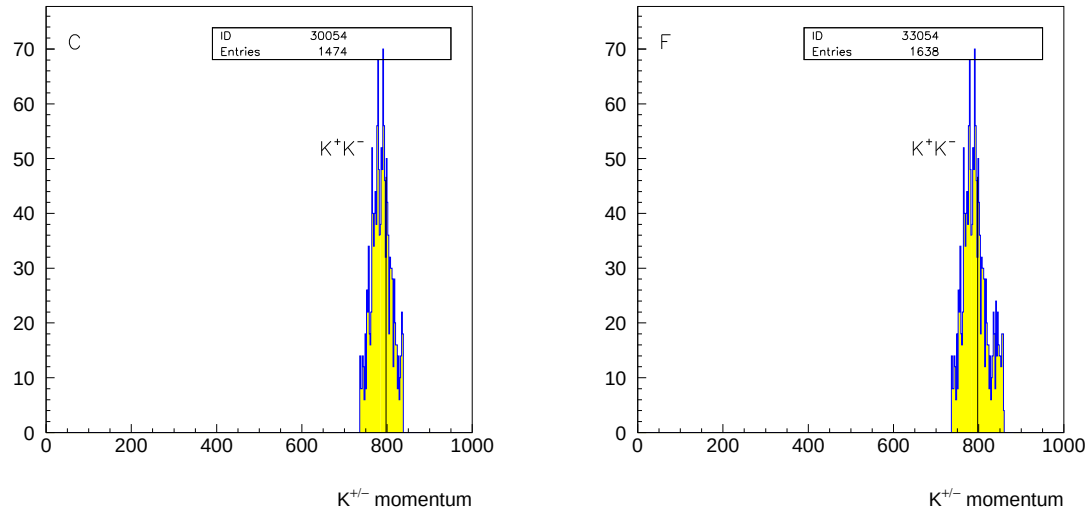

Figure 6.4: Momentum of two prongs. Each event causes one entry. Left region C and right region F (see table 6.1).

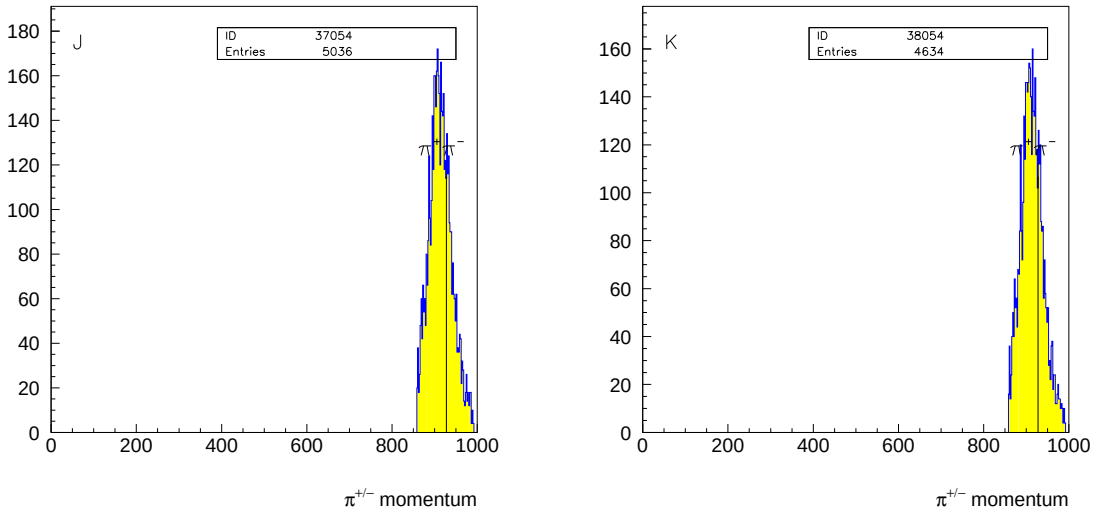

Figure 6.5: Momentum of two prongs. Each event causes one entry. Left region J and right region K (see table 6.1).

6.2 $\pi^+\pi^-$ Monte Carlo events

The $\pi^+\pi^-$ Monte Carlo events are produced as usual.

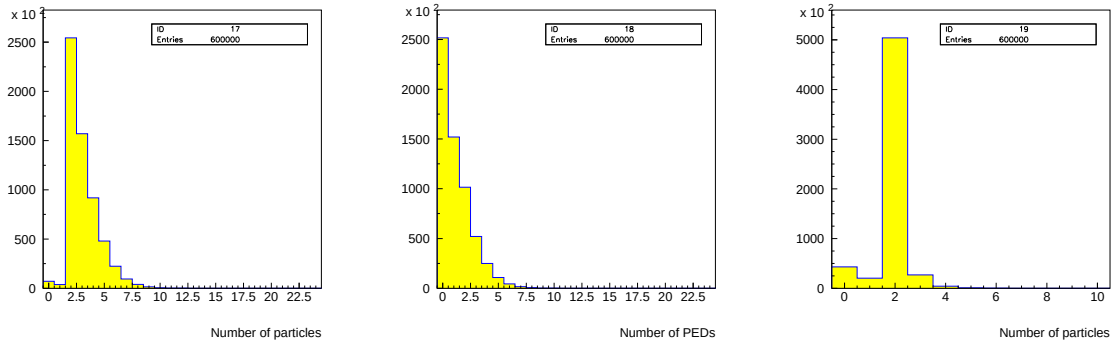

Figure 6.6: The number of particles, PEDs and charged tracks for Monte Carlo events. 600 000 produced Monte Carlo $\pi^+\pi^-$ events are represented in each histogram.

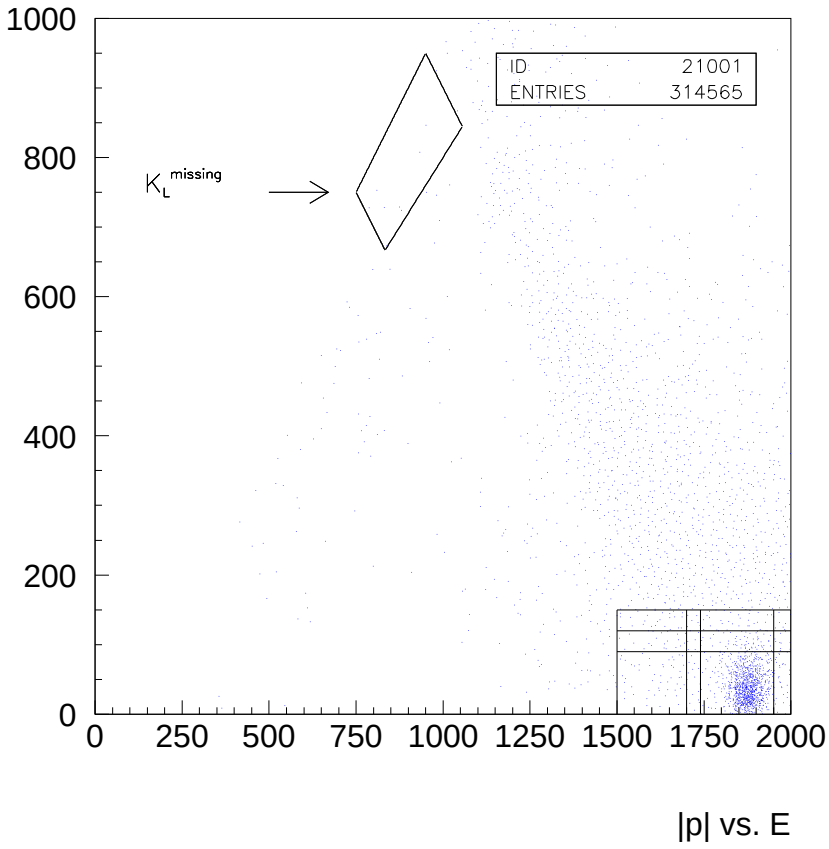

Figure 6.7: $|\vec{p}|$ vs. E. the kinematical regions are defined in table 6.1.

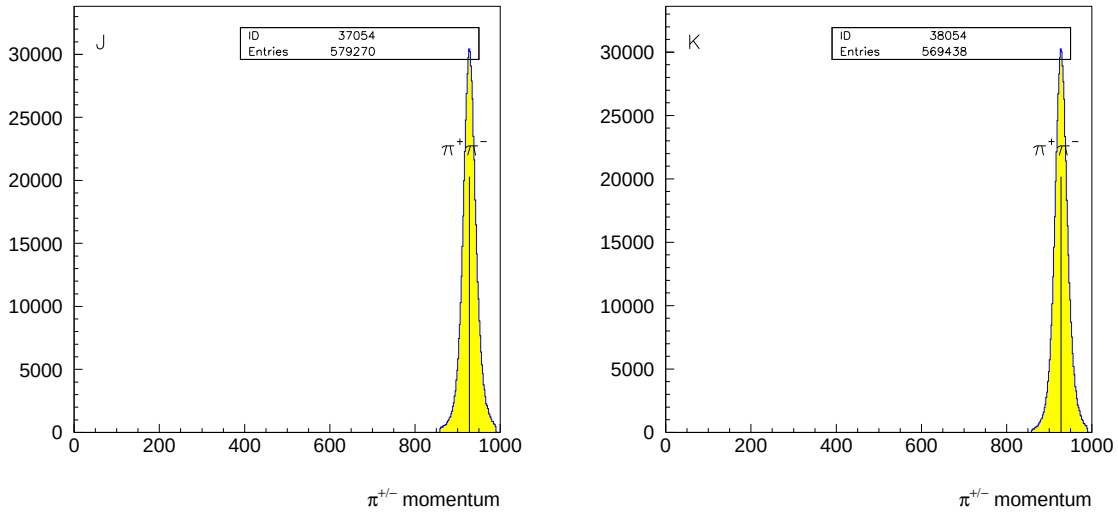

Figure 6.8: Momentum of two prongs. Each event causes one entry per event. Left region J and right region K (see table 6.1).

6.3 K^+K^- Monte Carlo events

The K^+K^- Monte Carlo events are produced as usual.

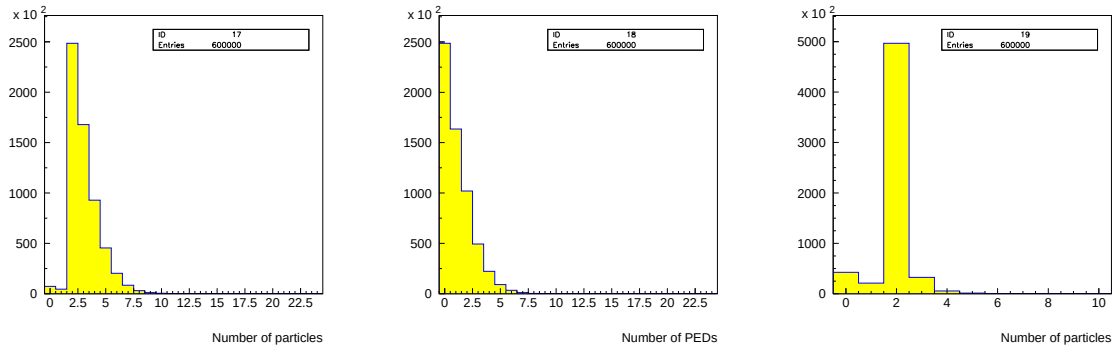

Figure 6.9: The number of particles, PEDs and charged tracks for Monte Carlo events. 600 000 produced Monte Carlo K^+K^- events are represented in each histogram.

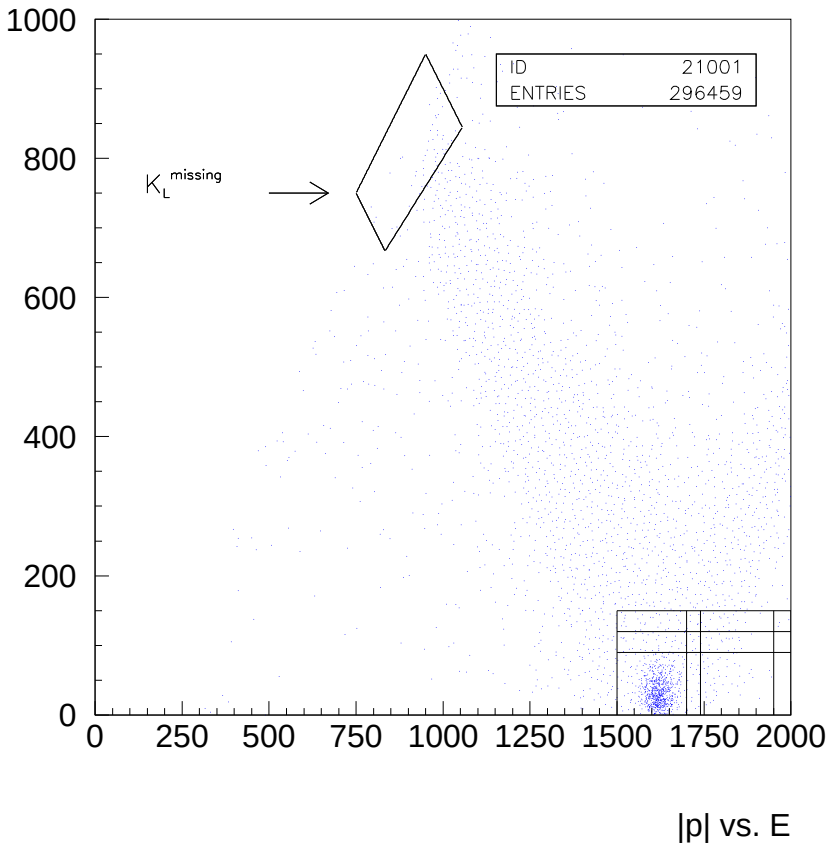

Figure 6.10: $|\vec{p}|$ vs. E. the kinematical regions are defined in table 6.1.

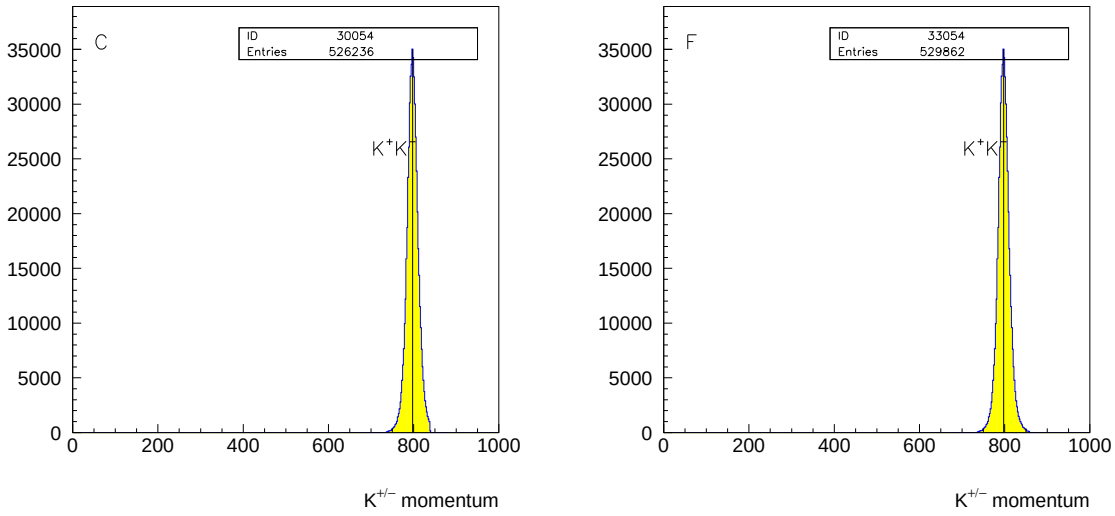

Figure 6.11: Momentum of two prongs. Each event causes one entry per event. Left region C and right region F (see table 6.1).

6.4 The Branching Ratios

Now the branching ratios for the 2-prong data will be discussed. Again formula 5.5 is used. Here no corrections due to Monte Carlo production of the events is needed.

region	$\#(\pi^+\pi^-)$	#(rec. MC)	$BR(\bar{\mathrm{p}}\mathrm{p} \to \pi^+\pi^-)$
G	2 407	281 266	$(3.350 \pm 0.183) \cdot 10^{-3}$
H	2 227	277 371	$(3.143 \pm 0.172) \cdot 10^{-3}$
I	1 850	263 728	$(2.746 \pm 0.153) \cdot 10^{-3}$
J	2 518	289 635	$(3.404 \pm 0.185) \cdot 10^{-3}$
K	2 317	284 719	$(3.186 \pm 0.174) \cdot 10^{-3}$
L	1 916	269 184	$(2.787 \pm 0.155) \cdot 10^{-3}$

Table 6.2: $\pi^+\pi^-$ branching ratios.

region	$\#(\mathrm{K}^+\mathrm{K}^-)$	#(rec. MC)	$BR(\bar{\mathrm{p}}\mathrm{p} \to \mathrm{K}^+\mathrm{K}^-)$
A	881	271 188	$(1.272 \pm 0.077) \cdot 10^{-3}$
B	834	269 559	$(1.211 \pm 0.074) \cdot 10^{-3}$
C	737	263 118	$(1.097 \pm 0.069) \cdot 10^{-3}$
D	995	274 419	$(1.420 \pm 0.085) \cdot 10^{-3}$
E	932	272 296	$(1.340 \pm 0.081) \cdot 10^{-3}$
F	819	264 931	$(1.210 \pm 0.074) \cdot 10^{-3}$

Table 6.3: $\mathrm{K}^+\mathrm{K}^-$ branching ratios.

From these results the following branching ratios can be determined in the same way as in section 5.7.

A comparison between real data and Monte Carlo events proves that the regions J and K are the right ones for the determination of the $\pi^+\pi^-$ branching ratio. For $\mathrm{K}^+\mathrm{K}^-$ final state it is region C.

$$BR(\bar{\mathrm{p}}\mathrm{p}(\mathrm{LH}_2) \to \pi^+\pi^-) = (3.30 \pm 0.20) \cdot 10^{-3} \tag{6.1}$$

$$BR(\bar{\mathrm{p}}\mathrm{p}(\mathrm{LH}_2) \to \mathrm{K}^+\mathrm{K}^-) = (1.10 \pm 0.07) \cdot 10^{-3} \tag{6.2}$$

Chapter 7

Summary

Table 7.1 summarizes the results derived in this report. The values are also compared to previous Crystal Barrel publications and the OBELIX experiment.

$\bar{p}p \rightarrow$	target	BR		
		this report	CB publications	OBELIX
$\pi^0\pi^0$	LH_2	$(6.14 \pm 0.40) \cdot 10^{-4}$	$(6.93 \pm 0.43) \cdot 10^{-4}$ [2]	$(2.8 \pm 0.4) \cdot 10^{-4}$ [6]
$\pi^0\eta$	LH_2	$(2.71 \pm 0.30) \cdot 10^{-4}$	$(2.12 \pm 0.12) \cdot 10^{-4}$ [2]	
K_LK_S	LH_2	$(8.64 \pm 1.02) \cdot 10^{-4}$	$(9.0 \pm 0.6) \cdot 10^{-4}$ [7]	$(7.8 \pm 0.8) \cdot 10^{-4}$ [8]
$\pi^+\pi^-$	LH_2	$(3.30 \pm 0.20) \cdot 10^{-3}$	$(3.07 \pm 0.13) \cdot 10^{-3}$ [2]	
K^+K^-	LH_2	$(1.10 \pm 0.07) \cdot 10^{-3}$	$(0.99 \pm 0.05) \cdot 10^{-3}$ [2]	

Table 7.1: Summary of the results. The K_LK_S braching ratio is obtained from $K_S \rightarrow \pi^0\pi^0$ decay in our experiment, whereas OBELIX detects the $\pi^+\pi^-$ decay mode.

The summary shows a good agreement between the former Crystal Barrel results and the values derived in this report. The large discrepancy between our value for the $\pi^0\pi^0$ branching ratio and the corresponding OBELIX value is still unresolved. But our K_SK_L value agrees with OBELIX result. They measured K_L's decaying into $\pi^+\pi^-$ whereas we looked for the $\pi^0\pi^0$ deacy mode.

This accordance may be a hint for a reason of the large discrepancy of the $\pi^0\pi^0$ branching ratios. Their K_LK_S branching ratio is independent on their determined γ detection efficiency in contrast to the $\pi^0\pi^0$ value.

Appendix A

Another analysis done by Mario Herz

On our meeting at October 27/28 1997 Eberhard Klempt presented branching ratios of two body final states that had been analysed by Mario Herz [10]. Unfortunately, he used the same data set that had already been used in the ealier analysis [2]. Here I only want to remind you of Mario's results which have been extracted from his tranparencies.

In contrast to the analysis introduced in this report there a kinematic fit was applied. The results are normalised to the number of all neutral annihilations in minimum bias data. He found $(3.14 \pm 0.25)\%$ for LH_2 and$(3.16 \pm 0.28)\%$ for GH_2. As well as I, he looked for 4-γ final states. The K_L interaction probability he used was 42.8%.

Table A.1 summarizes his results.

$\bar{p}p \rightarrow$	target	BR
$\pi^0\pi^0$	LH_2	$(6.48 \pm 0.55) \cdot 10^{-4}$
$\pi^0\eta$	LH_2	$(1.82 \pm 0.15) \cdot 10^{-4}$
K_LK_S	LH_2	$(7.9 \pm 1.2) \cdot 10^{-4}$
$\pi^0\pi^0$	GH_2	$(1.65 \pm 0.14) \cdot 10^{-3}$
$\pi^0\eta$	GH_2	$(0.48 \pm 0.04) \cdot 10^{-3}$
K_LK_S	GH_2	$(4.98 \pm 0.53) \cdot 10^{-4}$

Table A.1: Branching ratios analysed by Mario Herz

The main branching ratios for $\pi^0\pi^0$ are in good agreement. This supports the reliability of the Crystal Barrel result in contrast to the OBELIX value of $(2.8 \pm 0.4) \cdot 10^{-4}$.

Appendix B

Plots

In this appendix a plot for every determed branching ratio will be shown. In adddition the values are summarized in table B.1. Table B.2 gives branching ratios for target densities not supported by the Crystal Barrel experiment.

$\bar{p}p \rightarrow$	LH_2	GH_2 (12 atm)
$\pi^0\pi^0$	$(6.14 \pm 0.40) \cdot 10^{-4}$	$(1.49 \pm 0.08) \cdot 10^{-3}$ [1]
	$(6.93 \pm 0.43) \cdot 10^{-4}$ [2]	
	$(2.8 \pm 0.4) \cdot 10^{-4}$ OBELIX [6]	
$\pi^0\eta$	$(2.71 \pm 0.30) \cdot 10^{-4}$	$(5.52 \pm 0.40) \cdot 10^{-4}$ [1]
	$(2.12 \pm 0.12) \cdot 10^{-4}$ [2]	
$K_L K_S$	$(8.64 \pm 1.02) \cdot 10^{-4}$	$(6.83 \pm 0.71) \cdot 10^{-4}$[1]
$K_S \rightarrow \pi^0\pi^0$	$(9.0 \pm 0.6) \cdot 10^{-4}$[7]	
$K_S \rightarrow \pi^+\pi^-$	$(7.80 \pm 0.76) \cdot 10^{-4}$ OBELIX [8]	
$\pi^+\pi^-$	$(3.30 \pm 0.20) \cdot 10^{-3}$	$(8.93 \pm 0.21) \cdot 10^{-1}$ [1]
	$(3.07 \pm 0.13) \cdot 10^{-3}$ [2]	
	$(3.20 \pm 0.30) \cdot 10^{-3}$ Bubble Chamber [16]	
K^+K^-	$(1.10 \pm 0.07) \cdot 10^{-3}$	$(8.80 \pm 0.54) \cdot 10^{-4}$ [1]
	$(0.99 \pm 0.05) \cdot 10^{-3}$ [2]	
	$(1.10 \pm 0.10) \cdot 10^{-3}$ Bubble Chamber [16]	

Table B.1: Branching ratios. The upper values are based on Crystal Barrel data, the lower values below the lines are determed by other research groups.

$\bar{p}p \rightarrow$	density	BR
$\pi^0\pi^0$	1	$(1.27 \pm 0.21) \cdot 10^{-3}$ OBELIX [11]
$\pi^0\pi^0$	0.0012	$(2.4 \pm 0.22) \cdot 10^{-3}$ derived ASTERIX [17]
$K_L K_S$	1	$(3.50 \pm 0.54) \cdot 10^{-4}$ OBELIX [8] ($K_S \rightarrow \pi^+\pi^-$)
$K_L K_S$	1	$(3.60 \pm 0.60) \cdot 10^{-4}$ ASTERIX [12]
$K_L K_S$	0.005	$(1.00 \pm 0.32) \cdot 10^{-4}$ OBELIX [8] ($K_S \rightarrow \pi^+\pi^-$)
$\pi^+\pi^-$	1	$(4.30 \pm 0.14) \cdot 10^{-3}$ ASTERIX [13]
$\pi^+\pi^-$	1	$(4.27 \pm 0.23) \cdot 10^{-3}$ OBELIX [14]
$\pi^+\pi^-$	0.05	$(4.26 \pm 0.11) \cdot 10^{-3}$ OBELIX [15]
K^+K^-	1	$(6.92 \pm 0.41) \cdot 10^{-4}$ ASTERIX [13]

Table B.2: Branching ratios for $\bar{p}p$ annihilation at rest for target densities not used in the Crystal Barrel experiment.
The very low pressure point for $\pi^0\pi^0$ was derived from the Asterix value for the $\pi^+\pi^-$ branching ratio measured with X-rays in coincidence. This is a pure P-state value and so is expected to be the branching ratio which would be measured at very low pressures - assuming that they are pure P-state, which is not too bad an approximation.

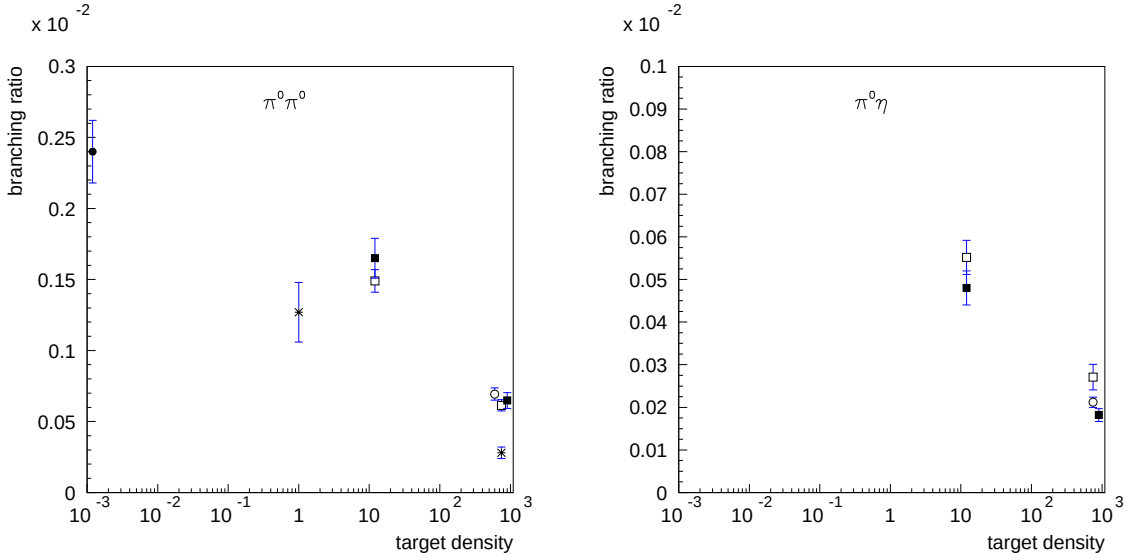

Figure B.1: (left) $\pi^0\pi^0$ branching ratio for different target densities. The two lower values were published by the OBELIX Collaboration ($\star$).
(right) $\pi^0\eta$ branching ratio.
$\square$ CB this report and [1]; $\circ$ CB [2]; $\blacksquare$ CB appendix A; $\star$ OBELIX [6] and [11] and $\bullet$ ASTERIX [17].

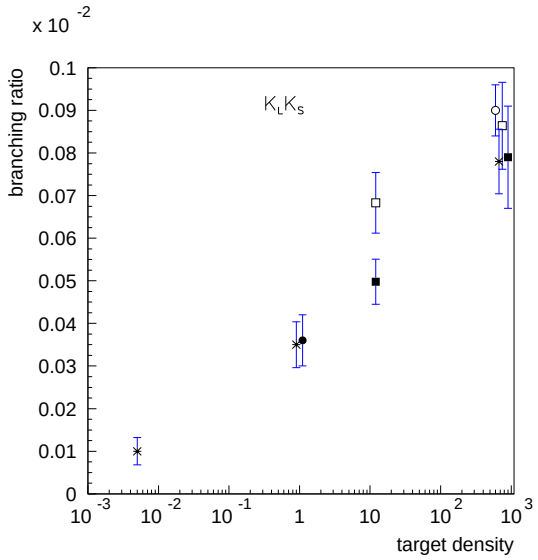

Figure B.2: K_LK_S branching ratios.
□ CB this report and [1]; ○ CB [7]; ■ CB appendix A; ⋆ OBELIX [8] and • ASTERIX [12]

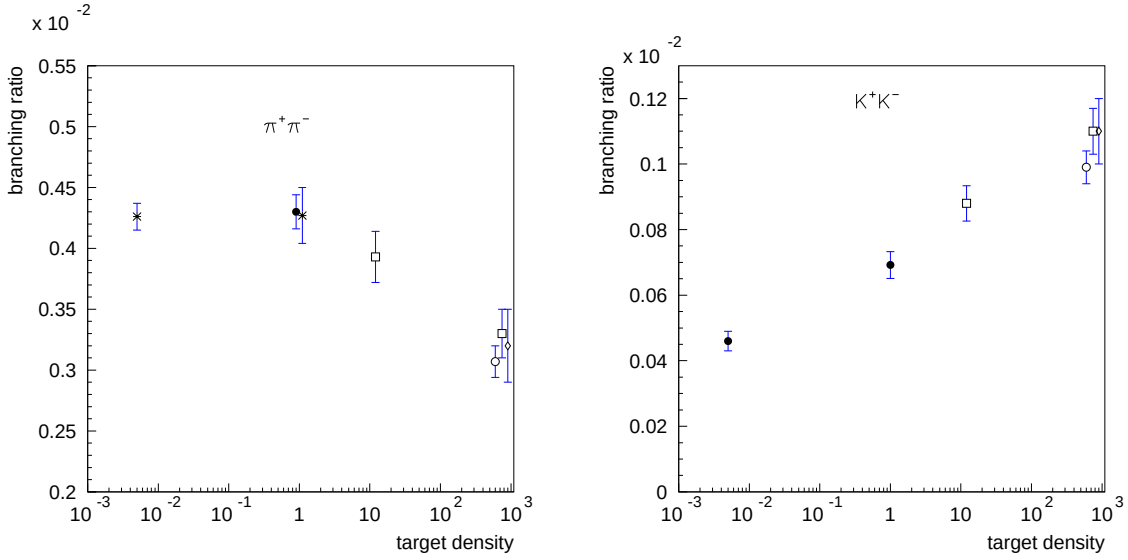

Figure B.3: (left) $\pi^+\pi^-$ branching ratio
(right) K^+K^- branching ratio
□ CB this report and [1]; ○ CB [7]; ⋆ OBELIX [14], [15]; • ASTERIX [13] and ◇ bubble chamber [16]

Bibliography

[1] CB-Note 345
B. Pick
Technical Report: $\bar{p}p$ annihilationn at rest into two-body final stats and branching ratios (GH_2)
Bonn, 1999

[2] The Crystal Barrel Collaboration, (C. Amsler et al.)
Z. Phys. **C58** (1993) 175-189
Antiproton-proton annihilation at rest into two-body final states

[3] M Merkel
Proton-Antiproton-Vernichtung in Ruhe in π^0X, ηX und ωX mit X= π^0, η und η'
Dissertation universität Mainz, 1993

[4] CB-Note 185, Version 2
M. Burchell
Analysis Writeup on $BR(\bar{p}p \to \pi^+\pi^-)$, $BR(\bar{p}p \to K^+K^-)$
(Annihilation at rest in LH_2) CERN 1992

[5] O. Cramer
Protoniumvernichtung in K_LK_S
Diplomarbeit Universität München, 1993

[6] OBELIX Collaboration, A. Zoccoli
HADRON97

[7] The Crystal Barrel Collaboration, (C. Amsler et al.)
Obervation of radiative $\bar{p}p$ annihilation into a ϕ meson
Phys. Lett. **B** 346 (1995) 363 - 370

[8] OBELIX Collaboration (A. Bertin et al.)
Protonium annihilation into K_LK_S at three different target densities
Phys. Lett. **B** 386 (1996) 486 - 494

[9] Review of Particle Properties
Phys. Rev. **D54**(1996)

[10] M. Herz, E. Klempt
Crystal Barrel Collaboration Meeting

Talk: Two-Body-Branching Ratios from $\bar{p}p$-annihilation at rest
27/28 October 1997 at CERN

[11] OBELIX Collaboration (M.Angelo et al.)
Phys. Lett. **B** 337 (1994)

[12] ASTERIX Collaboration (M. Doser et al.)
Phys. Lett. **B** 215 (1998) 792

[13] ASTERIX Collaboration (M. Doser et al.)
Nucl. Phys. **A** 486 (1988) 493

[14] OBELIX Collaboration (V.G. Ableev et al.)
Nuovo Cim. **A** 107 (1994) 2837

[15] OBELIX Collaboration (V.G. Ableev et al.)
Phys. Lett. B 329 (1994) 407

[16] C. Baltay et al.
Phys. Rev. Lett. 15 (1965) 532 (Bubble Chamber)

[17] Chris Batty
private communication